Global mercury records from natural archives reveal ecosystem responses to changing atmospheric deposition

Qinqin Chen[1,2], Qingru Wu[1,2], Yuying Cui[1,2], Shuxiao Wang[1,2,3*]

[1] State Key Joint Laboratory of Environmental Simulation and Pollution Control, School of Environment, Tsinghua University, Beijing, 100080, China
[2] State Environmental Protection Key Laboratory of Sources and Control of Air Pollution Complex, Beijing, 100084, China
[3] Lead contact
*Correspondence: shxwang@tsinghua.edu.cn

ABSTRACT

Global ecosystems face mercury contamination, yet long-term data is scarce, hindering understanding of ecosystem responses to atmospheric Hg input changes and policy evaluation. To address this gap, this study compiled a global mercury accumulation flux database using 221 cores from peat, lake, ice, and marine deposits. From 1700 to 2012, global averaged fluxes in peat, lake, ice, and marine deposits increased five-fold, six-fold, six-fold, and eight-fold, respectively. Notably, lake and peat mercury fluxes generally mirrored trends in total atmospheric mercury deposition modelled by GEOS-Chem and thus can reflect policy effects. For instance, the decreases of lake and peat mercury fluxes post-1950 in Europe evidenced effective environmental policies, while rises in East Asia-Oceania highlighted coal-use impacts, *inter alia*. Conversely, mercury fluxes in marine sediments and high-altitude natural deposits did not correspond well with atmospheric deposition, emphasising natural influences over anthropogenic impacts. Our study underscores these key regions and ecosystems for future mercury management.

Keywords: Mercury pollution, palaeoecology, natural deposits, GEOS-Chem, ecosystem recovery, policy evaluation

INTRODUCTION

As one of the top ten global pollutants, mercury (Hg) is notorious for its high toxicity and ability to bioaccumulate [1]. Mercury is mobilized by anthropogenic activities such as metal mining and fossil fuel burning [2,3], and natural activities such as volcanic eruptions and biomass burning, as well as reemissions from legacy Hg [1]. The emitted Hg exists primarily in a gaseous form (Hg^0) and can travel over long distances. During transport, Hg^0 may be oxidised to bio-accumulative and water-soluble forms, e.g., Hg^{2+} and methylmercury, and subsequently deposited to terrestrial ecosystems and oceans through dry and wet deposition processes. The deposited Hg eventually accumulated in environmental compartments like aquatic sediments and glaciers [1], contaminating ecosystems [4] and posing potential risks to humans [5]. To address the adverse effects of Hg, the Minamata Convention on Mercury, an international legally binding treaty, came into force in 2017 [6]. The convention complements national atmospheric protection policies like the UK's Clean Air Acts of 1956 and the US's Clean Air Acts of 1970, among the earliest regulations that could synergistically reduce Hg emissions through end-of-pipe controls.

Due to these pollution control efforts, recent observations showed reduced Hg emissions and concentrations in regions like the Arctic [7], Europe, and North America [8-10]. However, these reductions might not fully indicate changes in contamination levels within ecosystems. Ecosystems include various elements like organisms, waterbodies, and natural deposits, each governed by unique Hg deposition mechanisms. Of particular concern and research interest are natural deposits, including peat, lake sediments, marine sediments, and ice, as they serve as final Hg sinks and potential Hg sources of the respective ecosystems. These natural deposits inherently preserve and accumulate environmental contaminants like Hg in chronological order [11-13] and thus are known as natural archives. In particular, the Hg accumulated in nature archives in undisturbed regions was considered to be primarily sourced from atmospheric depositions [14]. Therefore, such long-term natural archive Hg records are valuable for studying how respective ecosystems, particularly their natural deposit component, respond to changing atmospheric Hg deposition.

Different types of natural archives may not respond the same to the changing inputs due to unique Hg deposition processes (see details in SI Table S1). For instance, Hg in peat accumulates from atmospheric deposition including vegetation fixation [15-19] and is influenced by peat growth and microbial decomposition [20]. In lake sediments, Hg accumulates from direct atmospheric deposition and catchment runoff, including legacy Hg from catchment soil [21-23]. Marine sediments acquire Hg through the balance of atmospheric deposition and reemissions, with waterbodies [24] and sea ice as natural barriers for Hg

exchange [25]. Coastal erosion can also contribute to Hg inputs in marine sediments [26]. Hg in ice results from atmospheric deposition, with significant photoreduction [27], sublimation and melting [27-29] causing annual deposition loss. Previous studies reviewed Hg records from natural archives like peat and lake sediments and offered qualitative assessments at regional and hemispheric scales [30-33] (see SI Supporting Text 1). However, these studies were limited in providing quantitative comparisons across ecosystems and regions. Such comparisons would be invaluable for understanding different ecosystem responses, evaluating the effectiveness of source-control policies, and informing future mitigation strategies.

In this study, we aim to utilize global Hg records from natural archives and atmospheric modelling to understand how different ecosystems, at least their natural deposit components acting as the Hg sink, respond to changing atmospheric Hg deposition. Firstly, we compiled a global natural archive Hg database from 1700 to 2012, assisted with General Additive Model (GAM). The database compiled Hg accumulation fluxes of 221 cores extracted from ice, peat, lake, and marine deposits that were primarily influenced by atmospheric Hg depositions. Secondly, the trend, changing rate, and magnitude of the Hg accumulation fluxes in the four types of natural archives were compared to the respective total atmospheric Hg deposition modelled by GEOS-Chem during the overlapped period from 1980 to 2012. This comparison served to elucidate how Hg accumulation levels change in natural archives in response to varying atmospheric Hg input. Finally, we investigated the four types of natural archive Hg records across eight key regions from 1700 to 2012. This investigation facilitated the evaluation of the effectiveness of past environmental policies and identified key regions and ecosystems that may require more targeted Hg management strategies.

RESULTS AND DISCUSSION

Global Natural Archive Mercury Database 1700-2012

We meticulously selected 221 cores primarily impacted by atmospheric Hg deposition, as indicated in the relevant literature (Fig. 1a, see detailed Method in Supporting Text 2, SI Fig. S1, and Dataset S1). The core selection was based on five stringent criteria, including the requirements that the core be free from significant physical and chemical disturbances, and that the core provided Hg accumulation data in flux ($mg/m^2/yr$) and possessed a temporal resolution of data points finer than 20 years, considering potential chronological errors. These selected cores were categorized into eight key regions, with the highest core numbers in North America (47%), followed by Europe (11%), the Arctic (11%, mainly Greenland), Latin America (9%, mainly Central America and the western Andes), Central Asia (8%, mainly Tibetan Plateau), East Asia (6%), Central and Southern Africa (3%), and Oceania (2%) (see SI Table S2 for a

full list). In terms of core types, 72% were lake cores (distributed globally), followed by peat cores (13%, mainly in Europe), marine cores (11%, in continental shelf areas), and ice cores (4%, in polar and mountainous regions).

Cores from different studies have varying temporal scales. The inconsistent temporal scales would impact the accuracy of regional synthesised data, which were generated by averaging the Hg accumulation flux data within each region annually. To address this problem, we employed GAM to predict Hg fluxes to 2012 for cores with shorter temporal scales, ensuring temporal consistency. We fed GAM with selected eight predictors: local anthropogenic emissions, local non-anthropogenic emissions (i.e., natural emissions and re-emissions), global total emissions, surface temperature, precipitation, and greenness fraction, elevations (or depths for marine cores), and the ratio between catchment area and lake area (see details in Table S4). The GAM analysis established correlations between predictors and each of the four types of natural archive Hg accumulation fluxes, which are the dependent variables. The four correlations explained 65%, 88%, 85%, and 83% of the deviances in lake cores, peat cores, marine cores and ice cores, respectively (Table 1). Based on the four correlations, a total of 31% of the Hg accumulation flux data from natural archives between 1980-2012 were predicted.

Combining the Hg accumulation flux data extracted from literature and GAM prediction, we compiled a global natural archive Hg database from 1700 to 2012 (referred to as "the database"). The database showed distinctive patterns of Hg accumulation fluxes in the four types of natural archives over the last three centuries. The global averaged Hg fluxes in peat, lake, ice, and marine cores, hereafter referred to as "peat-Hg fluxes", "lake-Hg fluxes", "ice-Hg fluxes", and "marine-Hg fluxes", have increased by five-fold, six-fold, six-fold, and eight-fold, respectively, culminating in peak contemporary levels at 0.033 ± 0.034 mg/m²/year, 0.055 ± 0.123 mg/m²/year, 0.001 ± 0.004 mg/m²/year, and 0.124 ± 0.175 mg/m²/year (mean ± standard deviation, SI Fig. S2-3, and SI Table S3). These substantial variations in changing rates and magnitudes highlight the differences among Hg deposition mechanisms in ice, peat, lake sediments and marine sediments. These differences reflect the key responses of the Hg sink within each ecosystem to the changing atmospheric Hg deposition. Therefore, the following section further discusses these responses, analysing the deviances and similarities between natural archive Hg accumulation and total atmospheric Hg deposition, leveraging data from the short yet critical overlapping periods.

Comparison between natural archive records and total atmospheric deposition (1980-2012)

To understand how Hg accumulation levels in natural archives change in response to varying atmospheric Hg input, a comparison was conducted between natural archive Hg records and

total atmospheric deposition modelled by GEOS-chem during the overlapping period of 1980-2012. The GEOS-chem model was driven by EDGAR anthropogenic Hg emissions [34] and MERRA2 meteorological data [35]. The modelling generated atmospheric Hg deposition fluxes (total, wet, and dry) in 2°×2.5° grids, an economical resolution for global simulation balancing modelling accuracy and computational cost. The modelling results were validated with observations, showing an acceptable error range of around 50% (SI Fig. S4). We compared the trends, changing rates, and magnitudes of the Hg accumulation fluxes in natural archives to the modelled total atmospheric Hg deposition fluxes at each coring area (Fig. 1b) and in eight key regions using regional synthesised data (Table 2).

For lake and peat cores, we found that 45% of lake-Hg fluxes and 46% of peat-Hg fluxes between 1980 and 2012 were within a one-fold range of their respective modelled total atmospheric deposition fluxes, indicating a good agreement in magnitudes. Extremes were noted, however, with 7% of lake-Hg fluxes (11 cores) and 7% of peat-Hg fluxes (2 cores) deviating by more than ten-fold. In such cases, lake-Hg and peat-Hg fluxes tend to surpass the modelled deposition (SI Fig. S5). We also found concordance in trends between the modelled atmospheric deposition and lake/peat-Hg fluxes in most regions. Exceptions were only found in regions where trends were statistically insignificant ($p > 0.05$) or where trends were generated with fewer cores (< 5). Additionally, we also found similar changing rates between lake/peat-Hg fluxes and the modelled atmospheric deposition in Europe, but changing rates in other regions differed by two to three-fold, with greater disparities in regions with fewer cores.

Such general concordance in trends between the modelled atmospheric deposition and lake/peat-Hg fluxes indicates that factors driving atmospheric deposition levels, such as emission control policies, are also likely the key drivers of lake-Hg and peat-Hg fluxes. This observation is further supported by the earlier established correlations by GAM analysis (SI Fig. S6-10). The correlation results revealed that local anthropogenic Hg emissions imposed the most significant impact on lake-Hg and peat-Hg fluxes, as evidenced by the highest F values among other factors (Table 1). Nevertheless, environmental factors like temperature and elevation also exerted significant effects on lake-Hg and peat-Hg fluxes. Temperature variations could influence lake-Hg and peat-Hg fluxes by impacting the biogeochemical cycles of Hg within lake and peat ecosystems. For instance, rising temperatures promoted vegetation growth and aquatic system productivity, leading to an increase in the input of organic matter-bound Hg to peat and lake sediments [18,36]. Besides, rising temperatures could contribute to glacier retreat, providing additional Hg input from meltwater to proglacial lakes [29,37,38]. Similarly, elevation could affect the atmospheric Hg supply to lake and peat ecosystems, as the formation and deposition of Hg^{2+} were found to increase with rising altitudes due to the increased availability of oxidants and intensified photochemical reactions [39-42] (see SI

Supporting Text 3 and Table S1 for further discussion on impact factors). These natural impacts partly explained the differences in changing rates and magnitudes between the modelled atmospheric deposition and lake/peat-Hg fluxes.

By contrast, marine-Hg and ice-Hg fluxes largely differed from the modelled atmospheric deposition in trends and displayed significant differences in changing rates and magnitudes. Notably, comparing magnitudes across the dataset, 58% of marine-Hg fluxes and 66% of ice-Hg fluxes between 1980 and 2012 showed disparities exceeding ten-fold, with only 19% of marine-Hg fluxes and 10% of the ice-Hg fluxes falling within the one-fold range of the respective total atmospheric Hg deposition fluxes. In general, marine-Hg fluxes were around 20-fold greater than the modelled deposition, while ice-Hg fluxes were around nine-fold smaller than the modelled deposition (SI Fig. S5).

The stark differences between ice/marine-Hg fluxes and modelled atmospheric deposition suggest that factors driving the change in atmospheric deposition, such as emission control policies, are not the primary drivers of ice-Hg or marine-Hg. This observation is also supported by the established correlations by GAM analysis, which revealed that the F values of local Hg emissions were not the highest, indicating they are not the primary drivers for ice-Hg or marine-Hg fluxes (SI Fig. S11-14). Instead, elevation/depth was found to have exerted the most significant impacts. For ice cores, higher elevations correlate with heightened ultraviolet intensity, which could linearly influence the photoreduction process of mercury in ice deposits [43], thus leading to the loss of deposited Hg. For marine cores, ocean depth could alter the marine-Hg fluxes by influencing the physical movement of marine sediments, to which Hg binds. These movements include sediment focusing [44] and sediment export to the deep sea [45,46]. Besides, surface temperature could significantly affect ice-Hg and marine-Hg fluxes by influencing the surrounding environment. For example, rising temperatures could result in the retreat of ice and glaciers in mountains [47,48] and sea surface [25] and could stimulate organism production, particularly in coastal marine environments [49]. These processes can modify the biogeochemical cycling of Hg, including its preservation, exchange and subsequently the Hg accumulation levels in ice and marine cores (see SI Supporting Text 3 for more discussion).

Overall, the evaluation of trends, changing rates, and magnitudes from 1980 to 2012 suggests that the Hg accumulation fluxes in lake and peat cores are likely to change along with atmospheric Hg inputs. The general concordance in trend, albeit with higher magnitudes, implies that lake and peat cores hold promise for assessing the influence of anthropogenic activities that can alter atmospheric Hg deposition levels. These activities include the commencement of major Hg emission sources and the implementation of emission-control

policies, spanning a broader historical range from 1700 to 2012. In contrast, Hg accumulation fluxes in marine and ice cores may not necessarily correspond to changes in atmospheric inputs. However, they can provide a contrasting perspective which could inform future policy-making regarding effective ecosystem recovery from Hg contamination. Through analysing the short-term overlapping data, the above findings have furnished us with the requisite characteristics of individual natural archives to better comprehend the change in levels of Hg records across the world over the past three centuries.

Spatial-temporal variations of natural archive mercury records (1700-2012)

Lake and peat cores marked the impacts of anthropogenic activities

In the 18th and 19th centuries, most lake-Hg and peat-Hg fluxes showed background levels of Hg accumulation (Fig. 2). Exceptions are lake-Hg fluxes in North America (1850 onwards), Central Asia (before 1850) and Latin America (1800-1900) (Fig. 2a-c). Lake-Hg fluxes in these areas were elevated potentially corresponding to the controversial high Hg emissions from silver, mercury, and gold mining [2,50] during the Spanish colonization (1570-1850) and Gold Rush era (1800 onwards). The natural archive evidence aligns with the findings of previous reviews [32,51], which concluded that Hg emissions from mining activities were only of local impact and/or overestimated (See SI Supporting Text 4 for discussion of atmospheric Hg emissions from mining activities).

From 1900 onwards, lake-Hg and peat-Hg fluxes in all regions started to rise, but their trajectories diverged after the 1950s. In Europe (Fig. 2d), the lake-Hg and peat-Hg fluxes reduced by 94% and 97%, respectively, from the respective peaks in the 1950s and 1970s to 2012. The fluxes in 2012 dropped to 0.039 [0.026, 0.052] (mean [CI2.5%, CI97.5%]) mg/m^2/year in lake cores and 0.022 [0.014, 0.030] mg/m^2/year in peat cores. These magnitudes closely resemble preindustrial levels, where the lake-Hg flux was 0.027 [0.015, 0.039] mg/m^2/year in 1866 and peat-Hg flux was 0.006 [0.004, 0.008] mg/m^2/year in 1760 (the earliest year with more than one core). The significant reductions observed in lake and peat cores in the most recent period align well with the decreasing trends of modelled total atmospheric Hg depositions during 1980-2012 (Table 2 and SI Fig. S15) and observed Hg^0 concentration and Hg^{2+} wet deposition during 1990-2010 [10]. The concurrent decreases could be largely attributed to the effective implementation of environmental policies aimed at reducing general air pollutant emissions from coal burning. These policies can be traced back to the United Kingdom's Clean Air Act 1956 prompted by the Great London Smog, and strengthened by a series of policies promulgated in the European Union region since 1970 [52]. Consequently, most European countries have since gradually decoupled their economic development and coal consumption (SI Fig. S16). Therefore, such reductions in lake-Hg and peat-Hg fluxes stand as

compelling evidence of the effective recovery of terrestrial ecosystems of lakes and peatlands, at least their natural deposit components, in Europe from Hg contamination as a result of effective policy controls.

In North America, lake-Hg fluxes initially showed a growth rate of 1.8% per year before the 1970s. Subsequently, the trend pivoted coincidently with the enactment of the Clean Air Act of 1970 in the United States, followed by a statistically insignificant decrease. The lake-Hg flux reached 0.023 [0.021, 0.025] mg/m²/year in 2012, a five-fold enrichment from the preindustrial level of 0.005 [0.0042, 0.0061] mg/m²/year in the year 1700. The post-1970 trend observed in peat-Hg fluxes also showed an insignificant decreasing trend mirroring that of lake-Hg fluxes. These overall insignificant decreasing trends in North America result from diverse changing patterns of lake-Hg and peat-Hg trends at subregions of North America. Fig. 3 illustrates the spatial-temporal changes of Hg accumulation in North America, expressed in partial effects. The spatial-temporal partial effects reveal changes in Hg accumulation fluxes over time and space and were also generated by GAM analysis (See SI Supporting Text 2 for methods). The result showed declining Hg accumulation fluxes on the eastern and western sides of North America, and increasing Hg accumulation fluxes with slowing year-on-year changing rates in the central region during 1980-2012. These ununiformed subregional trends from natural archives align with the general decreasing patterns in wet deposition observed in the eastern and western regions of the United States, alongside the increasing [53] or slowing decreasing trends [10] in the central region depending on targeted periods. Overall, the general statistically insignificant decreasing trends of lake-Hg and peat-Hg fluxes in North America are a contrast to the significant reductions in Europe. The differences are likely due to the United States' strong economic reliance on coal until 2008 as opposed to European countries' early decoupling (SI Fig. S16) and a contribution from transboundary Hg pollution across continents [53].

Unlike the declines in Europe and North America, lake-Hg fluxes in Oceania, central and southern Africa, and East Asia have experienced intensified Hg accumulation fluxes up until 2012 (Fig. 2e-h). The recent increasing lake-Hg fluxes agree with the modelled atmospheric deposition during 1980-2012. Both were likely driven by escalated coal usage in Australia, South Africa, and China, which rose by 71%, 190%, and 533% [54], respectively, over the same period. Contributions to these increases could also arise from Artisanal and Small-Scale Gold Mining (ASGM) activities, the largest contemporary emission source [1]. Triggered in part by surging gold prices after the 2000s, ASGM proliferated in developing regions worldwide, including central and southern Africa and China [55,56]. However, the magnitude of ASGM emissions carries substantial uncertainties and needs further validation (see SI Supporting Text 4 for more discussion). The rising trends in these areas are anticipated to persist, primarily due to the slow decoupling of economic growth and coal use (SI Fig. S16) and the

increasing gold production, partly from ASGM, in these regions [55]. Notably, these three regions displayed gradually increasing positive partial effects during 1980-2012 with East Asia standing out as an intensified Hg accumulation hotspot (SI Fig. S17).

Cores with unique changes indicate key regions and ecosystems for future management

Ice-Hg fluxes in Central Asia remained constant from the 18th century to the 1930s and then increased rapidly until 1960. Afterwards, the fluxes fluctuated greatly around 0.001 mg/m²/year to 2012. The post-1960 trend of Ice-Hg fluxes differed from that of the potential emissions impacting Central Asia, an extensive mountainous region spanning the Third Pole area. This region was influenced by global mercury emissions, particularly from East Asia and South Asia, both of which exhibited increasing trends [57]. In contrast, Hg fluxes in high-altitude lakes in the region accord with such rising emission trends as expected based on our analysis in the preceded section, standing at 0.020 [0.013, 0.027] mg/m^2/year in 2012. Nonetheless, the high-altitude lake-Hg fluxes had a year-on-year changing rate of 1.3%/year, which surpassed the modelled atmospheric deposition rate of 0.7% at lake locations during 1980-2012. The acceleration in the changing rate of lake-Hg fluxes in Central Asia could be due to a heightened atmospheric supply of oxidated Hg^{2+} at higher elevations [40,42]. Besides, if the lakes are proglacial, they also receive historical Hg inputs from glacier meltwater, which are enhanced by rising temperatures [29,38]. The glacier melting may also contribute to the fluctuated ice-Hg fluxes [28], yet more ice cores in this region are needed to improve the trend analysis as the current core number is not enough to provide convincing evidence. Nonetheless, these ice-lake dynamics underscore challenges in containing Hg contamination in high-altitude regions.

All marine-Hg fluxes maintained the increasing momentum, including those in Europe. The marine cores in Europe showed an insignificant increasing trend. This non-decreasing trend contrasts sharply with the region's declining lake-Hg and peat-Hg fluxes, both of which nearly returned to their respective preindustrial levels. The marine-Hg fluxes here only decelerated from 3%/year to 0.4%/year after the 1960s, lagging slightly behind the peak times of lake and peat-Hg fluxes. The marine-Hg fluxes reached 0.144 [0.140, 0.148] mg/m^2/year in 2012, ranking among the highest levels within the database. Similarly, the marine-Hg fluxes in the Arctic showed significant monotonical increasing trends from 1920 to 2012; although the growth rate decreased from 2.8%/year to 0.6%/year before and after 1980. This contemporary increasing trend contrasts with the region's decreasing ambient atmospheric Hg concentration by -0.95%/year since 1995 (data from Station Alert at the northern tip of Greenland) [7] and opposed to a decreasing modelled atmospheric deposition rate of -0.2%/year during 1980-2012 (averaged from marine core locations). The Arctic marine-Hg flux stood at 0.108 [0.077, 0.140] mg/m^2/year in 2012 and was marked as a Hg accumulation hotspot in Fig. 3. The sustained rises

in marine-Hg fluxes in both the Arctic and Europe are attributed to various factors, including Hg circling in the marine environment [58], continuous inputs from coastal erosion [26], and possible enhanced ecosystem productivity in coastal areas [36]. The Arctic region also receives additional inputs from melting Greenland glaciers and permafrost amplified by rising temperatures [59,60]. The increasing marine-Hg flux trends in the Arctic and Europe evidenced the delayed or limited responses of the marine ecosystems to changing atmospheric Hg deposition. We also acknowledge that the above analyses of marine cores are limited by their smaller numbers compared to peat and lake cores. Therefore, we encourage future studies to provide additional validation.

Conclusion

In summary, we compiled a global natural archive Hg record database spanning the years from 1700 to 2012, utilizing natural archive data from 221 cores from ice, peat, lake, and marine deposits across eight key regions. Our analysis focused on investigating how these natural deposits acting as Hg sinks of respective ecosystems respond to changes in total atmospheric Hg deposition. Our findings revealed that lake-Hg and peat-Hg fluxes exhibited a strong association with local anthropogenic Hg emissions, and mirrored the trend of total atmospheric Hg deposition, albeit with higher magnitudes. This distinct characteristic evidenced the positive effect of past collective policies in Europe in recovering lake and peat ecosystems, at least their sedimentary components, from Hg contamination. Additionally, it revealed elevated Hg accumulation in lake and peat ecosystems in East Asia and Oceania, likely driven by economic development, including coal consumption among other factors. Conversely, ice-Hg and marine-Hg fluxes were primarily regulated by natural processes, such as Hg photoreductions, ice melting, and coastal erosion, and thus were not sensitive to changing atmospheric inputs driven by anthropogenic interventions such as emission controls. As a result, we found universal rising trends in marine-Hg fluxes in Europe and the Arctic post the 1950s despite the declining atmospheric emissions, concentrations, and depositions. Additionally, our findings underscore the challenges in containing Hg contamination in ecosystems in high-altitude regions, due to the dynamic Hg exchange, including the remobilization of historical Hg through ice melting. This dynamic process adds complexity to managing Hg pollution in these regions.

Although natural deposits may not fully represent entire ecosystems, they do provide insight into the principal response from the Hg sink within these ecosystems, which could also serve as a potential Hg source. Therefore, our results carry significant implications, highlighting challenges for future Hg management in both terrestrial and marine ecosystems. Targeted mitigation strategies are essential, tailored to key ecosystems in oceans and high-altitude areas, as well as key regions such as East Asia, Oceania, Africa, and the Arctic. Besides, the changing

346 natural conditions of ecosystems, including variations in vegetation types, organism
347 productivity, and soil erosion levels, can also influence Hg contamination levels. This linkage
348 emphasises the importance of addressing Hg pollution and tackling climate change in tandem
349 [61]. Additionally, more paleoenvironmental studies are needed in less-explored natural archive
350 materials, such as ice and marine sediments, and in less-explored regions, particularly Asia,
351 South America, and Africa, to support effectiveness assessments of Hg mitigation policies,
352 particularly the Minamata Convention on Mercury.

353 To push forward research in this direction, in future applications, the established global natural
354 archive Hg database 1700-2012 could potentially help to 1) reconstruct long-time-scale, global-
355 gridded, atmospheric Hg depositions, which could be achieved by combining and
356 complementing natural archive Hg records (long temporal scale but limited in special coverage)
357 and global modelled gridded depositions (global coverage but limited in temporal scales).
358 Successful reconstruction can provide valuable Hg data for less studied areas such as East Asia,
359 Africa and South Asia; 2) incorporate with global Hg cycle modelling to constrain Hg emission
360 estimates, including anthropogenic emissions from sources like metal mining, and aquatic
361 reemissions; 3) disentangle climate and socio-economic drivers of Hg accumulation fluxes in
362 the identified key ecosystems, i.e., marine and high altitude lake systems and generate more
363 targeted policies and measures for effective ecosystem recovery from Hg contamination.

METHODS

We conducted this study following the below processes (Fig. 4), for the detailed method, please see SI Supporting Text 2:

1) Data preparation of natural archive Hg records and atmospheric Hg deposition: (a) Compiled a database using geochemical data from lake, peat, marine, and ice cores. (b) Modelled total atmospheric Hg deposition at respective coring locations using GEOS-Chem.
2) Analysed the disparities between natural archive Hg records and modelled total atmospheric Hg deposition by magnitude, trend, and changing rate: (a) comparing at each coring location and (b) comparing the regional synthesised data in the eight defined regions.
3) Spatial-temporal analysis of natural archive Hg records across the globe over the past three centuries: (a) analysed impacts of key anthropogenic activities, including environmental policies, on different natural archives over time. (b) identified key regions and ecosystems to inform future policy-making regarding reducing Hg contamination levels.

This study employed a multidisciplinary approach from palaeoecology and atmospheric sciences, resulting in uncertainties that span various dimensions. Please refer to SI Supporting Text 4 for in-depth discussions. In essence, these uncertainties encompass, but are not limited to, the following aspects:

1) Potential bias stemming from core distribution and numbers, which could be more pronounced in regions like Southeast Asia, the Arctic, East Asia, central and southern Africa, and South America. Such bias may affect the accuracy of trend or magnitude analyses.
2) Uncertainties in natural archive Hg records arising from different deposition mechanisms. See SI Table S1 for a summary detailing pre- and post-depositional processes contributing to differences between natural archive Hg fluxes and atmospheric Hg deposition fluxes.
3) Uncertainties in natural archive Hg records arising from chronologies, including dating error range and difference in dating methods employed across studies. Consequently, the geochemical Hg records discussed herein should be understood as an approximate period of ± 10 years, rather than precise years.
4) Uncertainties in natural archive Hg records arising from the concentration-to-flux conversion. Contemporary Hg accumulation fluxes in ice and marine cores might be underestimated due to the consistent sedimentation rates used in the conversion.

5) Uncertainties in total atmospheric Hg deposition linked to the transport and deposition processes modelled in GEOS-chem. The model could potentially underestimate the total deposition onto the ice surface and overestimate it onto lakes due to uncertainties of high-altitude modelling and lake Hg reemissions, respectively. These uncertainties may influence the accuracy of magnitude comparison between the modelled and geochemical Hg fluxes.
6) Uncertainties in Hg emission estimates, including potential overestimation of emissions from 19th-century metal mining activities and more recent ASGM. The latter may further lead to an overestimated GEOS-chem-modelled atmospheric deposition in East Asia, central and southern Africa, and Latin America in 1980-2012.

RESOURCE AVAILABILITY

Materials availability

The natural archive Hg flux data and core information, including references, of the selected 221 cores are available in Dataset S1. Ground observation data of wet mercury deposition and concentrations are available in Dataset S2.

Data and code availability

The data used to plot Fig.1-3 are provided in Dataset S3. The GAM codes are available upon reasonable request to the lead contact Shuxiao Wang (shxwang@tsinghua.edu.cn).

SUPPLEMENTAL INFORMATION

Supporting Text 1-4

Fig. S1–S19

Table S1-S5

Dataset S1 to S3

ACKNOWLEDGEMENTS

We also want to give special thanks to William Shotyk, Eichler Anja, Sarah Roberts, James Zheng, Joe McConnell, Stefan Engels, Yuan Hezhong, and Takahiro Hosono, who kindly dug deep on their computers and provided us with precious raw data from their papers published ages ago. Some further suggested useful literature and capable researchers we should look into or contact, which are of great value. This paper and the database will not be as complete without their kind help.

Funding

This work was funded by the National Natural Science Foundation of China (2222604, 42394094), the International Postdoctoral Exchange Fellowship Program (Talent Introduction Program) (YJ20210103), the Shuimu Scholar Fellowship from Tsinghua University (2020SM075), and the Special fund of State Key Joint Laboratory of Environment Simulation and Pollution Control (22L02ESPC).

AUTHOR CONTRIBUTIONS

QC, QW and SW conceived the idea. QC compiled the natural archive Hg accumulation database, conducted the statistical analysis, performed GAM modelling, prepared drafts and all rounds of revisions of the manuscript. QW and SW provided expertise in interpreting results from Hg GEOS-chem modelling and GAM modelling, arranged the framework of the article, and provided important critiques. YC performed the GEOS-chem Hg deposition modelling and participated in the interpretation of the results. SW supervised the project and was in charge of the overall study. All authors contributed to the discussion, revision and edition of the manuscript.

DECLARATION OF INTERESTS

The authors declare no competing interests.

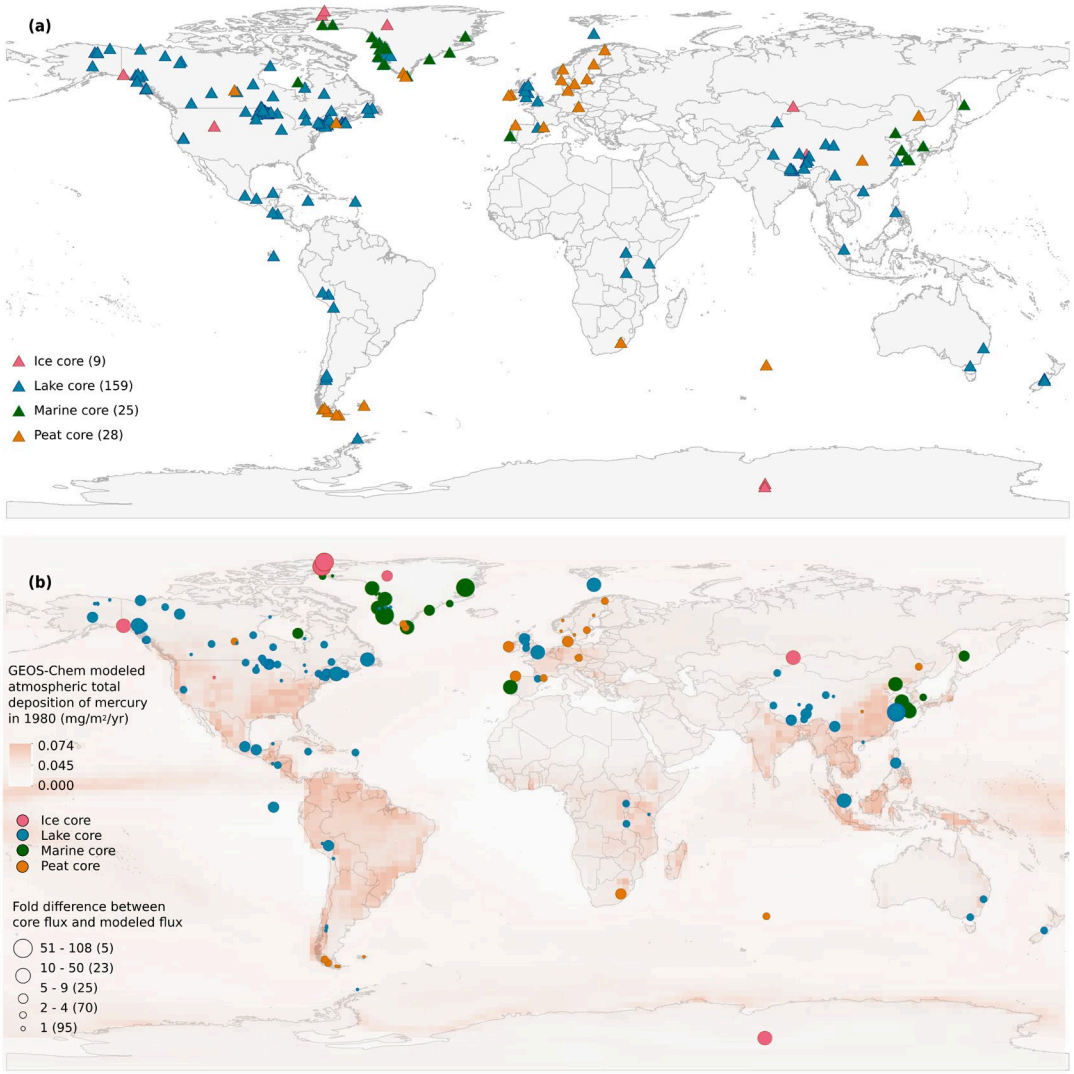

446

447 **Fig. 1** (a) Spatial distributions of natural archive records of Hg. The numbers in brackets represent
448 the number of cores from the respective natural archives compiled in the database. Note that some
449 cores collected from the same or nearby locations are not fully visible in the figure; please refer to
450 Dataset S1 for detailed core information. (b) A comparison between natural archive Hg fluxes and
451 total (wet + dry) atmospheric Hg deposition fluxes modelled by GEOS-Chem at each coring site in
452 the base year 1980, a year with the greatest number of cores. Larger circles indicate greater
453 disparities in magnitude. Generally, lake-Hg, peat-Hg, and marine-Hg fluxes are greater than the
454 modelled total atmospheric Hg deposition fluxes, while ice-Hg fluxes are smaller. A total of 42%
455 of the cores show good agreement with the modelled values, indicated by a difference within 1-fold.
456 However, 12% of the cores exhibit differences larger than 10-fold, mostly marine and ice cores.

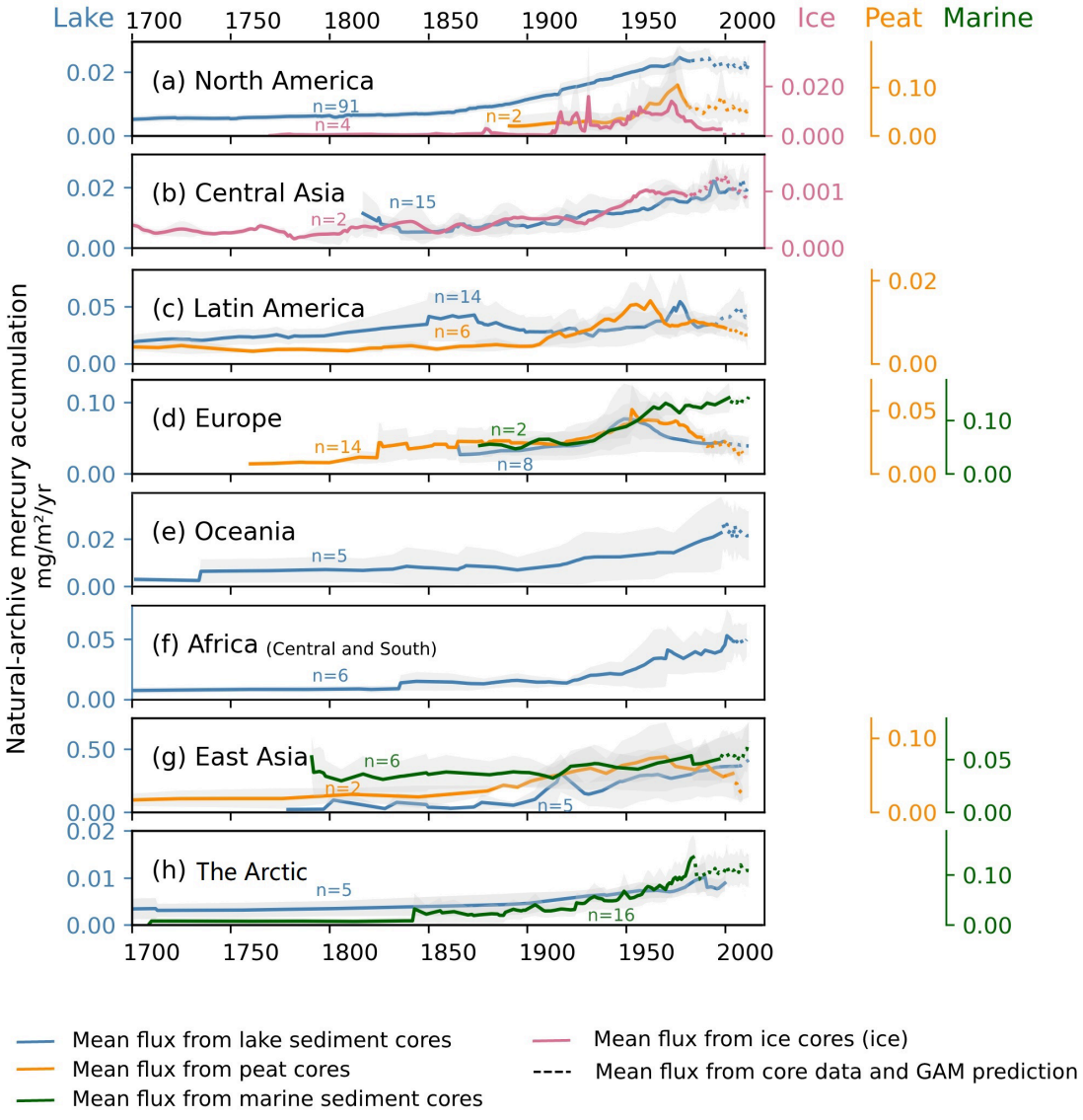

Fig. 2 The synthesised regional Hg accumulation fluxes reconstructed from ice, peat, lake sediments, and marine sediments from 1700 to 2012. In this context, Africa refers to central and southern areas, Oceania covers Australia and New Zealand, Latin America covers Mexico and the western Andes area, and the Arctic represents Greenland and nearby islands. The shaded areas represent 95% confidence intervals, and '*n*' next to each line indicates the maximum number of cores used in plotting. Here only plotted the fluxes that were averaged from two or more cores. Dotted extended lines indicate that the fluxes were calculated using both core data and predicted values generated by the General Additive Model (GAM). The use of core + GAM predicted data aims to avoid errors induced by inconsistent numbers of cores each year, particularly after 2000, when the number of cores decreased significantly.

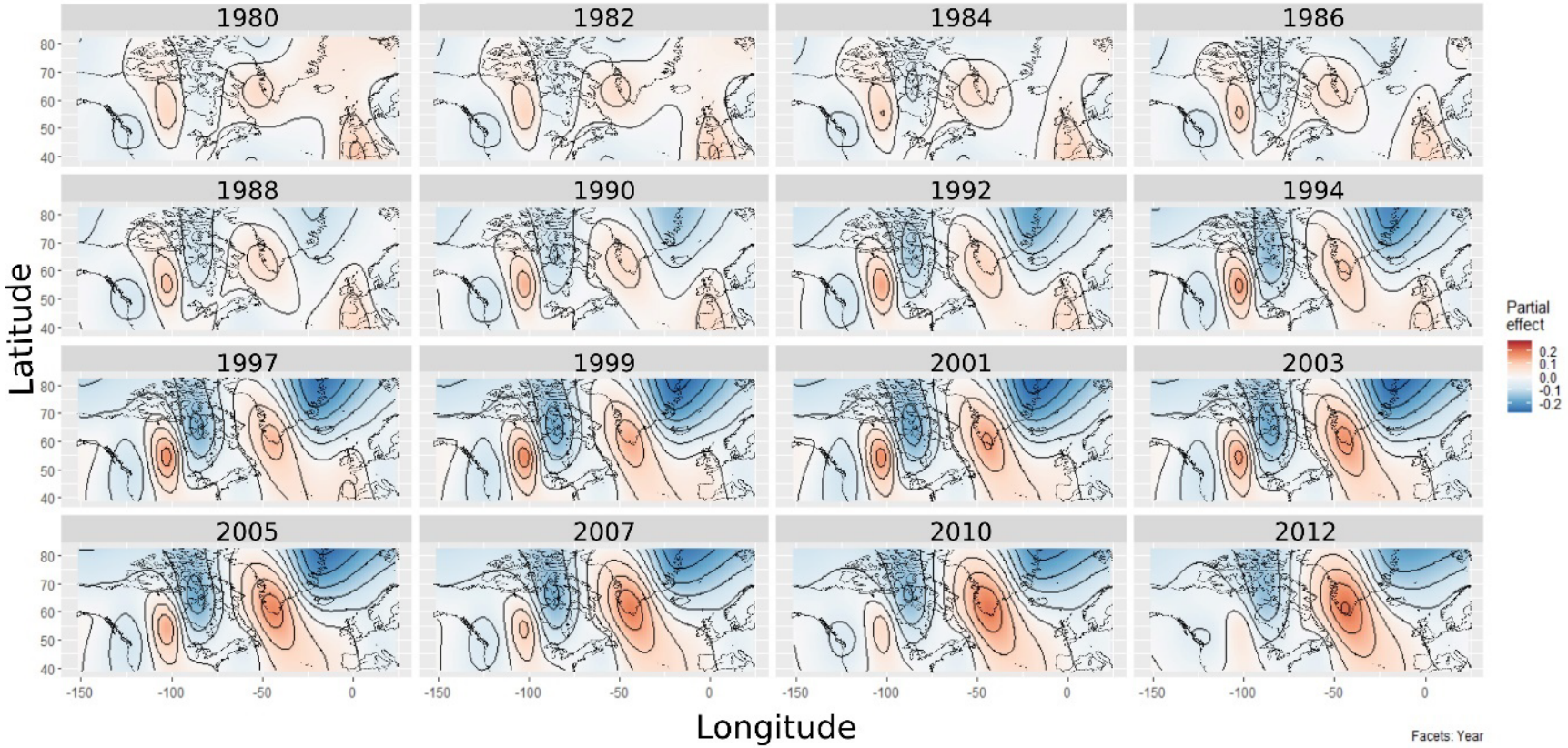

Fig. 3 Spatial-temporal variations in natural archive data of Hg accumulation fluxes denoted as partial effects, across North America (104 cores with 93% being lake cores), the Arctic (24 cores with 67% being marine cores), and Europe (24 cores with 58% being peat cores and 33% lake cores) from 1980 to 2012, analyzed using GAM. The plots were overlaid with map contours spanning the coordinates 38N-82N, 150W-23E. The change of partial effects visually demonstrates how Hg accumulation fluxes at specific locations change along with time while holding other variables constant. This spatial-temporal GAM analysis does not distinguish between core types, aiming for a comprehensive comparison among ecosystems and geographical locations. Note that lake and peat cores are more likely to mirror total atmospheric deposition compared to marine cores. The result of this regional analysis aligns with that of the global analysis (SI Fig. S17); both results show decreasing accumulation fluxes in Europe (terrestrial environment), increasing fluxes in the Arctic region (marine environment), and mixed effects in North America (terrestrial environment).

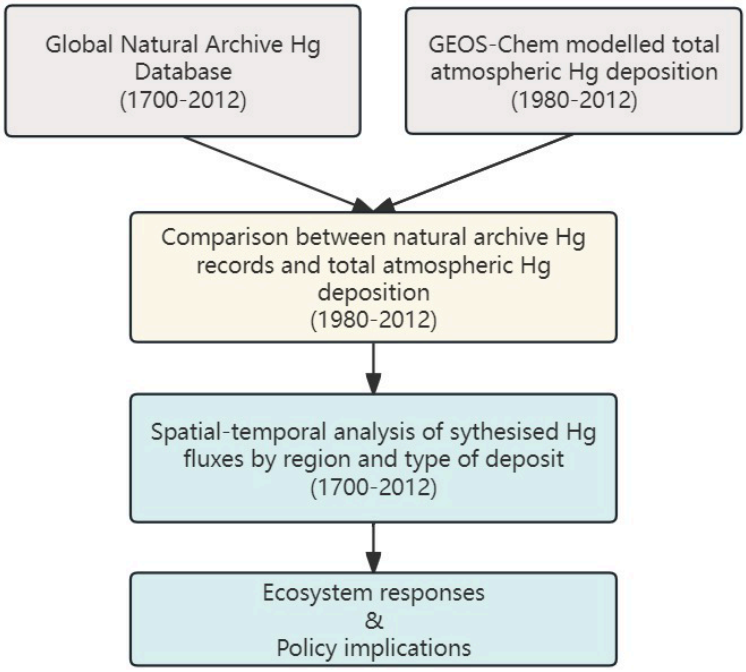

478

479 **Fig. 4** The workflow of this study, encompassing three steps. Step 1: Data preparation for
480 natural archive Hg records and atmospheric Hg deposition (grey boxes). Step 2: Comparative
481 analysis of the data from Step 1 to assess disparities during the overlapping period of 1980-
482 2012, aiming to understand the response of Hg accumulation in natural deposits acting as the
483 Hg sinks of respective ecosystems to changing atmospheric Hg inputs (yellow box). Step 3:
484 Spatial-temporal analysis of natural archive Hg records spanning three centuries, integrating
485 insights from Step 2 to identify key ecosystems and regions for future management (green
486 boxes).

Table 1 Database summary and impacts of individual changing factors on the respective natural archive Hg fluxes using general additive modelling (GAM). Star signs represent significant levels of the impacts of variables on the respective natural archive Hg records; three stars represent a level of 0.001, two stars represent a level of 0.01, and one star represents a level of 0.05. A minus sign indicates that the variable does not apply to the respective core type. Numbers in parentheses are F values. A higher F value indicates a higher effect of the variable on the respective natural archive Hg records. For graphic display see SI Figs. S7-14.

Core type	Number of cores in the database	Geographic factors		Environmental factors			Emission-related factors			Deviance explained
		Elevation/ Ocean depth	Catchment area vs. lake area	Temperature	Precipitation	Greenness fraction	Local anthropogenic emission	Local non-anthropogenic emission	Global total emission	
Lake core	159	*** (36.10)	*** (62.32)	*** (60.74)	*** (5.53)	*** (37.09)	*** (76.10)	*** (37.13)	(0.00)	65.0%
Peat core	28	*** (27.32)	-	*** (16.51)	** (1.02)	*** (16.74)	*** (30.32)	*** (8.13)	*** (5.38)	88.1%
Marine core	25	*** (120.48)	-	*** (15.27)	(0.00)	-	*** (46.63)	(0.70)	(0.00)	85.2%
Ice core	9	*** (6.26)	-	*** (2.98)	(0.00)	-	-	*** (1.82)	** (1.08)	83.0%
Total	221									

Table 2 Spatial comparison between natural archive data of Hg accumulation fluxes and modelled total atmospheric Hg deposition fluxes (in brackets) by trend, changing rate, and magnitude. Modelled results were extracted from respective coring locations and were presented in brackets for easy comparison. ↑ indicates a general increasing trend, ↓ indicates a general decreasing trend. * indicates the trend is at a significance level of 0.05.

Core type	North America	Europe	Latin America	Oceania	Central and Southern Africa	Central Asia	East Asia	The Arctic
Trend from 1980 to 2012								
Lake core	↓ (↑*)	↓*(↓*)	↑*(↑*)	↑*(↑*)	↑*(↑*)	↑*(↑*)	↑*(↑*)	↑*(↑)
Peat core	↓ (↑*)	↓*(↓*)	↓*(↑)				↓*(↑*)	
Ice core	↓ (↑*)					↑(↑*)		
Marine core		↑(↑)					↑(↑*)	↑*(↓)
Changing rate %/year from 1980 to 2012								
Lake core	-0.3 (0.3)	-1.7 (-1.6)	0.4 (0.6)	1.1 (0.6)	2.2(0.8)	1.3 (0.7)	1.9 (3.7)	2.2 (0.2)
Peat core	-0.2 (0.4)	-0.4 (-0.6)	-0.6 (0.3)				-0.9 (1.8)	
Ice core	-3.5 (0.5)					0.1 (0.7)		
Marine core		0.4 (0.8)					0.6 (1.9)	0.4 (-0.2)
Flux in 2012 (mg/m^2/year, mean [CI2.5%, CI97.5%])								
Lake core	0.023 [0.021,0.025] (0.014) ([0.014,0.016])	0.039 [0.026,0.052] (0.017) ([0.014,0.020])	0.034 [0.026,0.043] (0.024) ([0.018, 0.030])	0.021 [0.011,0.031] (0.018) ([0.011,0.026])	0.045 [0.036,0.055] (0.021) ([0.017,0.025])	0.020 [0.013,0.027] (0.010) ([0.008,0.012])	0.414 [0.119,0.709] (0.017) ([0.011,0.024])	0.007 [0.003,0.011] (0.007) ([0.006,0.009])
Peat core	0.054 [0.039,0.069] (0.011) ([0.000,0.037])	0.022 [0.014,0.030] (0.014) ([0.011,0.017])	0.010 [0.008,0.011] (0.017) ([0.012,0.022])				0.025 [0.015,0.034] (0.019) ([0.003,0.036])	
Ice core	0.0001 [0.0000,0.0001] (0.006) ([0.000,0.015])					0.001 [0.001,0.001] (0.007) ([0.000,0.030])		
Marine core		0.144 [0.140,0.148] (0.005) ([0.005,0.005])					0.067 [0.048,0.086] (0.006) ([0.003,0.010])	0.108 [0.077,0.140] (0.008) ([0.006,0.009])
Maximum core count								

Lake core	91	8	14	5	6	15	5	5
Peat core	2	14	6				2	
Ice core	4					2		
Marine core		2					6	16

496

REFERENCES

1. UNEP, *Global Mercury Assessment 2018*. 2019.
2. Streets, D.G., et al., *Total Mercury Released to the Environment by Human Activities.* Environmental Science & Technology, 2017. **51**(11): p. 5969-5977.
3. Streets, D.G., et al., *Historical releases of mercury to air, land, and water from coal combustion.* Science of The Total Environment, 2018. **615**: p. 131-140.
4. Wu, Q., et al., *Ecosystem Mercury Recovery and Health Benefit Under the Minamata Convention in a Changing Climate.* Reviews of Environmental Contamination and Toxicology, 2022. **260**(1): p. 15.
5. Zhang, Y.X., et al., *Global health effects of future atmospheric mercury emissions.* Nature Communications, 2021. **12**(1).
6. UNEP, *Minamata Convention on Mercury, Text and Annexes*. 2019.
7. MacSween, K., et al., *Updated trends for atmospheric mercury in the Arctic: 1995–2018.* Science of The Total Environment, 2022. **837**: p. 155802.
8. Giang, A. and N.E. Selin, *Benefits of mercury controls for the United States.* Proceedings of the National Academy of Sciences, 2016. **113**(2): p. 286-291.
9. Selin, H. and N.E. Selin, *From Stockholm to Minamata and beyond: Governing mercury pollution for a more sustainable future.* ONE EARTH, 2022. **5**(10): p. 1109-1125.
10. Zhang, Y., et al., *Observed decrease in atmospheric mercury explained by global decline in anthropogenic emissions.* Proceedings of the National Academy of Sciences, 2016. **113**(3): p. 526-531.
11. Jensen, A. and A. Jensen, *Historical deposition rates of mercury in scandinavia estimated by dating and measurement of mercury in cores of peat bogs.* Water Air & Soil Pollution, 1991. **56**(1): p. 769-777.
12. Benoit, J.M., W.F. Fitzgerald, and A.W.H. Damman, *The biogeochemistry of an ombrotrophic bog: Evaluation of use as an archive of atmospheric mercury deposition.* ENVIRONMENTAL RESEARCH, 1998. **78**(2): p. 118-133.
13. Percival, J.B. and P.M. Outridge, *A test of the stability of Cd, Cu, Hg, Pb and Zn profiles over two decades in lake sediments near the Flin Flon Smelter, Manitoba, Canada.* SCIENCE OF THE TOTAL ENVIRONMENT, 2013. **454**: p. 307-318.
14. Blais, J.M., M.R. Rosen, and J.P. Smol, *Environmental contaminants: Using natural archives to track sources and long-term trends of pollution*. Vol. 18. 2015: Springer.
15. Hansson, S.V., R. Bindler, and F. De Vleeschouwer, *Using Peat Records as Natural Archives of Past Atmospheric Metal Deposition.* Environmental Contaminants: Using Natural Archives to Track Sources and Long-Term Trends of Pollution, 2015. **18**: p. 323-354.
16. Norton, S.A., et al., *A comparative study of long-term Hg and Pb sediment archives.* Environmental Chemistry, 2016. **13**(3): p. 517-527.
17. Rausch, N., et al., *Retention of atmospheric Cu, Ni, Cd and Zn in an ombrotrophic peat profile near the Outokumpu Cu-Ni mine, SE-Finland.* JOURNAL DE PHYSIQUE IV, 2003. **107**: p. 1127-1130.
18. Zhou, J., et al., *Vegetation uptake of mercury and impacts on global cycling.* Nature Reviews Earth & Environment, 2021. **2**(4): p. 269-284.
19. Jiskra, M., et al., *A vegetation control on seasonal variations in global atmospheric mercury concentrations.* Nature Geoscience, 2018. **11**(4): p. 244-250.
20. Verbeke, B.A., et al., *Latitude, elevation, and mean annual temperature predict peat organic matter chemistry at a global scale.* Global Biogeochemical Cycles, 2022. **36**(2): p. e2021GB007057.
21. Shotbolt, L.A., A.D. Thomas, and S.M. Hutchinson, *The use of reservoir sediments as environmental archives of catchment inputs and atmospheric pollution.* Progress in Physical Geography, 2005. **29**(3): p. 337-361.

22. Roberts, S.L., et al., *Quantification of Spatial and Temporal Trends in Atmospheric Mercury Deposition across Canada over the Past 30 Years.* Environmental Science & Technology, 2021. **55**(23): p. 15766-15775.
23. Wiklund, J.A., et al., *Anthropogenic mercury deposition in Flin Flon Manitoba and the Experimental Lakes Area Ontario (Canada): A multi-lake sediment core reconstruction.* Science of The Total Environment, 2017. **586**: p. 685-695.
24. Lamborg, C.H., et al., *A global ocean inventory of anthropogenic mercury based on water column measurements.* Nature, 2014. **512**(7512): p. 65-68.
25. DiMento, B.P., et al., *The impact of sea ice on the air-sea exchange of mercury in the Arctic Ocean.* Deep Sea Research Part I: Oceanographic Research Papers, 2019. **144**: p. 28-38.
26. Meng, M., et al., *An Integrated Model for Input and Migration of Mercury in Chinese Coastal Sediments.* Environmental Science & Technology, 2019. **53**(5): p. 2460-2471.
27. Kang, S., et al., *Dramatic loss of glacier accumulation area on the Tibetan Plateau revealed by ice core tritium and mercury records.* The Cryosphere, 2015. **9**(3): p. 1213-1222.
28. Kang, S., et al., *Atmospheric Mercury Depositional Chronology Reconstructed from Lake Sediments and Ice Core in the Himalayas and Tibetan Plateau.* Environmental Science & Technology, 2016. **50**(6): p. 2859-2869.
29. Zhu, T., et al., *Accumulation of Pollutants in Proglacial Lake Sediments: Impacts of Glacial Meltwater and Anthropogenic Activities.* Environmental Science & Technology, 2020. **54**(13): p. 7901-7910.
30. Li, C., et al., *Unequal Anthropogenic Enrichment of Mercury in Earth's Northern and Southern Hemispheres.* ACS Earth and Space Chemistry, 2020. **4**(11): p. 2073-2081.
31. Goodsite, M.E., et al., *How well do environmental archives of atmospheric mercury deposition in the Arctic reproduce rates and trends depicted by atmospheric models and measurements?* Science of The Total Environment, 2013. **452-453**: p. 196-207.
32. Cooke, C.A., et al., *Environmental archives of atmospheric Hg deposition – A review.* Science of The Total Environment, 2020. **709**: p. 134800.
33. Lee, J.H., et al., *Spatiotemporal Characterization of Mercury Isotope Baselines and Anthropogenic Influences in Lake Sediment Cores.* Global Biogeochemical Cycles, 2021. **35**(10): p. e2020GB006904.
34. Muntean, M., et al., *Evaluating EDGARv4.tox2 speciated mercury emissions ex-post scenarios and their impacts on modelled global and regional wet deposition patterns.* Atmospheric Environment, 2018. **184**: p. 56-68.
35. Gelaro, R., et al., *The modern-era retrospective analysis for research and applications, version 2 (MERRA-2).* Journal of climate, 2017. **30**(14): p. 5419-5454.
36. Zhang, Y., et al., *An updated global mercury budget from a coupled atmosphere-land-ocean model: 40% more re-emissions buffer the effect of primary emission reductions.* One Earth, 2023. **6**(3): p. 316-325.
37. Perez-Rodriguez, M., et al., *Thawing of snow and ice caused extraordinary high and fast mercury fluxes to lake sediments in Antarctica.* GEOCHIMICA ET COSMOCHIMICA ACTA, 2019. **248**: p. 109-122.
38. Sun, X., et al., *Melting Himalayas and mercury export: Results of continuous observations from the Rongbuk Glacier on Mt. Everest and future insights.* Water Research, 2022. **218**: p. 118474.
39. Weigelt, A., et al., *Tropospheric mercury vertical profiles between 500 and 10 000 m in central Europe.* Atmospheric Chemistry and Physics, 2016. **16**(6): p. 4135-4146.
40. Yang, H., et al., *Historical Reconstruction of Mercury Pollution Across the Tibetan Plateau Using Lake Sediments.* Environmental Science & Technology, 2010. **44**(8): p. 2918-2924.
41. Zheng, J., *Archives of total mercury reconstructed with ice and snow from Greenland and the Canadian High Arctic.* Science of the Total Environment, 2015. **509**: p. 133-144.

42. Huang, J., et al., *Spatial distribution and magnification processes of mercury in snow from high-elevation glaciers in the Tibetan Plateau.* Atmospheric Environment, 2012. **46**: p. 140-146.
43. Mann, E.A., et al., *Mercury in Arctic snow: Quantifying the kinetics of photochemical oxidation and reduction.* SCIENCE OF THE TOTAL ENVIRONMENT, 2015. **509**: p. 115-132.
44. Thiagarajan, N. and J.F. McManus, *Productivity and sediment focusing in the Eastern Equatorial Pacific during the last 30,000 years.* Deep Sea Research Part I: Oceanographic Research Papers, 2019. **147**: p. 100-110.
45. Martin, J., et al., *Recent accumulation of trace metals in sediments at the DYFAMED site (Northwestern Mediterranean Sea).* MARINE POLLUTION BULLETIN, 2009. **59**(4-7): p. 146-153.
46. Cossa, D., et al., *Mediterranean Mercury Assessment 2022: An Updated Budget, Health Consequences, and Research Perspectives.* Environmental Science & Technology, 2022. **56**(7): p. 3840-3862.
47. Overeem, I., et al., *Substantial export of suspended sediment to the global oceans from glacial erosion in Greenland.* Nature Geoscience, 2017. **10**(11): p. 859-863.
48. Fox-Kemper, B., H.T. Hewitt, C. Xiao, G. Aðalgeirsdóttir, S.S. Drijfhout, T.L. Edwards, N.R. Golledge, M. Hemer, R.E. Kopp, G. Krinner, A. Mix, D. Notz, S. Nowicki, I.S. Nurhati, L. Ruiz, J.-B. Sallée, A.B.A. Slangen, and Y. Yu, *Ocean, Cryosphere and Sea Level Change*. Climate Change 2021: The Physical Science Basis. Contribution of Working Group I to the Sixth Assessment Report of the Intergovernmental Panel on Climate Change, ed. V. Masson-Delmotte, P. Zhai, A. Pirani, S.L. Connors, C. Péan, S. Berger, N. Caud, Y. Chen, L. Goldfarb, M.I. Gomis, M. Huang, K. Leitzell, E. Lonnoy, J.B.R. Matthews, T.K. Maycock, T. Waterfield, O. Yelekçi, R. Yu, and B. Zhou. 2021, Cambridge, United Kingdom and New York, NY, USA. 1211–1362.
49. Trombetta, T., et al., *Water temperature drives phytoplankton blooms in coastal waters.* PLOS ONE, 2019. **14**(4).
50. Camargo, J.A., *Contribution of Spanish–American silver mines (1570–1820) to the present high mercury concentrations in the global environment: a review.* Chemosphere, 2002. **48**(1): p. 51-57.
51. Engstrom, D.R., et al., *Atmospheric Hg Emissions from Preindustrial Gold and Silver Extraction in the Americas: A Reevaluation from Lake-Sediment Archives.* ENVIRONMENTAL SCIENCE & TECHNOLOGY, 2014. **48**(12): p. 6533-6543.
52. Crippa, M., et al., *Forty years of improvements in European air quality: regional policy-industry interactions with global impacts.* Atmospheric Chemistry and Physics, 2016. **16**(6): p. 3825-3841.
53. Weiss-Penzias, P.S., et al., *Trends in mercury wet deposition and mercury air concentrations across the U.S. and Canada.* Science of The Total Environment, 2016. **568**: p. 546-556.
54. bp, *bp Statistical Review of World Energy - all data*. 2022.
55. Verbrugge, B. and S. Geenen, *Global Gold Production Touching Ground: Expansion, Informalization, and Technological Innovation*. 2020, Cham: Springer International Publishing: Cham.
56. Veiga, M.M. and O. Fadina, *A review of the failed attempts to curb mercury use at artisanal gold mines and a proposed solution.* The Extractive Industries and Society, 2020. **7**(3): p. 1135-1146.
57. Yu, B., et al., *Tracing the Transboundary Transport of Mercury to the Tibetan Plateau Using Atmospheric Mercury Isotopes.* Environmental Science & Technology, 2022. **56**(3): p. 1568-1577.
58. Zhang, Y., et al., *Six centuries of changing oceanic mercury.* Global Biogeochemical Cycles, 2014. **28**(11): p. 1251-1261.
59. Dastoor, A., et al., *Arctic mercury cycling.* Nature Reviews Earth & Environment, 2022. **3**(4): p. 270-286.

60. Asmund, G. and S.P. Nielsen, *Mercury in dated Greenland marine sediments.* Science of The Total Environment, 2000. **245**(1): p. 61-72.
61. UNEP, *Chemicals, Wastes and Climate change: Interlinkages and Potential for Coordinated Action*. 2021.

Supporting Information for

Global mercury records from natural archives reveal ecosystem responses to changing atmospheric deposition

This PDF file includes:

Text 1 to 4

Figures S1 to S19

Tables S1 to S5

SI References

Other supporting materials for this manuscript include the following:

Datasets S1 to S3

Supporting information Text

Text 1. Comparative analysis between this study and other mercury pollution-related studies using natural archives

Several studies have examined mercury pollution using natural archives, encompassing global-scale reviews[1-3] and regional analyses such as those in the Americas[4] and the Arctic[5]. These studies address various topics, including understanding deposition mechanisms in natural archives, validating emissions from Artisanal and Small-Scale Gold Mining (ASGM), and comparing Hg accumulation levels between the northern and southern hemispheres. These studies share certain common traits. Firstly, they primarily offer qualitative analyses of impact factors. Secondly, the regional trends, if any, are typically illustrated by stacking plots of individual cores, making it challenging to generate general trends. Lastly, data comparisons often rely on trends and qualitative assessments.

This study builds upon previous reviews in several ways. Firstly, it employs quantitative analysis of impact factors using Generalized Additive Models (GAM). Secondly, it compares synthesised regional fluxes based on both trend and magnitude. This regional comparison is facilitated by specific processes, including careful core selection to ensure a similar base for reflecting atmospheric deposition, temporal interpolation for obtaining annual Hg fluxes, and GAM prediction to fill data gaps between 1980-2012 in individual cores.

Furthermore, this study comprehensively compared individual core data with the respective GEOS-Chem modelled total atmospheric mercury deposition from 1980 to 2012, examining trends, changing rates, and magnitudes. These comparisons provide insights into how natural archives respond to changing atmospheric total deposition, highlighting disparities between natural archive data and atmospheric deposition. Caution is thus advised in future studies when making inferences about atmospheric deposition and conducting comparisons with atmospheric emissions using natural archive data.

Lastly, despite serving different research purposes, our study collected and analysed a larger number of cores (221) compared to other reviews. The compiled raw flux data from individual cores and the synthesised regional flux data are publicly available (Dataset S1 and S3), offering valuable resources for advancing future research in the field.

Text 2. Methods

2.1 Database compilation of natural archive mercury records

Core selection for the database. To compile the Hg accumulation flux database, we focused on peer-reviewed journal papers published before August 2022 using the search engine Web of Science. The search was done by all keyword combinations between the pollutant (‘mercury’ OR ‘Hg’) and natural archives (‘lake sediment’ OR ‘marine sediment’ OR ‘lake’ OR ‘peat’ OR ‘peatland’ OR ‘sediment’ OR ‘ice’ OR ‘glacier’ OR ‘snow’ OR ‘soil’). We carefully selected papers and cores based on the following criteria:

1) The Hg preserved in cores was primarily sourced from atmospheric deposition. For instance, (a) we excluded cores from small lakes that receive sewage discharges, (b) excluded marine cores at estuaries directly receiving terrestrial river inputs, (c) preferably chose hydrologically closed lakes, and (d) preferably chose ombrotrophic (rainfed, thus only atmospheric input) peat cores or minerogenic peat with ombrotrophic characteristics than other kinds of peat cores.

2) Coring places were not disrupted by significant human activities, e.g., sediment cleaning and peat burning, or affected by natural geophysical processes, e.g., earthquakes, landslides, and hydrodynamic mixing of sediments.
3) Cores have no significant post-depositional movements, including diagenesis processes, as indicated in the papers. Note that this criterion relies solely on the assessment of the paper authors, which could contain errors. Furthermore, the absence of any mention of post-depositional movements in the papers does not necessarily imply the absence of such movements.
4) The disclosed Hg data include accumulation flux (mg/m^2/year) or the respective papers disclosed Hg concentration (mg/kg) together with other necessary archival information that enables the conversion from Hg concentrations to Hg fluxes.
5) The Hg fluxes were determined in a temporal resolution finer than 20 years, which is the approximated range of dating errors of lead-210[6] and carbon-14[7] in materials with ages ≤300 years, to avoid large chronological errors induced by dating techniques.

Data acquisition and compilation. After the selection, we focused on 221 cores and extracted the following data and information: (a) Hg-related data, including Hg flux and Hg concentration, (b) physical properties of cores, including chronology, sedimentation rate, and density, (c) environmental settings, including core coordinates, elevation, region and country, surrounding land cover, nearby Hg emission sources, and possible disturbances. (d) In the case of lake cores, we also collected data on catchment area, lake area and sediment-focusing factor if provided.

We obtained Hg flux data from (a) authors through email requests, (b) tables or SI database if provided in the papers, and (c) figures using WebPlotDigitizer (https://apps.automeris.io/wpd/), a free online tool for data extraction from figures, and (d) converted from concentration using eq1. Specifically, the concentration-to-flux conversion was applied to a total of 36 cores (16% of the total cores), they are three ice/snow cores, four peat cores, 10 lake cores, and 19 marine cores. To obtain the closest estimates of Hg fluxes from conversion (eq 1), we calculated sediment accumulation rates (kg-sed/m^2/yr) over different sedimentary sections if the papers provided with section parameters including core depths (m), age spans ($age_{section\text{-}top} - age_{section\text{-}bottom}$), and sediment densities (kg-sed/m^3). Otherwise, we adopted the disclosed full-core-averaged sedimentary accumulation rate to perform the conversion, which was mostly in marine cores.

$$Hg\ Flux = Hg\ Concentration \times sediment\ accumulation\ rate \quad \text{eq 1}$$

With the raw Hg flux data prepared, we used linear interpolation to fill gaps between years to obtain annual Hg flux data. The annual Hg accumulation flux data and respective core information were compiled into the Hg accumulation database (Dataset S1).

Database cross-check. We also conducted two rounds of data cross-checks. First, the data in the database were compared with data in respective papers to eliminate errors from manual data extraction. Second, we compared the flux data within the database to check the consistencies of core data in the same region, the same type of natural archive, and the same coring location to find erroneous values from published papers, which may be derived from human errors, including wrong unit used and wrong data disclosed. If found inconsistency, we contacted the corresponding authors of the papers to validate the published data. If we received authors' updates, we replaced the wrong data with the updated one in our database; if no response was received as some papers were published decades ago, we removed the data from our database. Eventually, we gathered and compiled Hg deposition flux data from 221 cores in 70 papers, covering eight regions and 34 countries and subregions from 1700 to 2012.

2.2 GEOS-Chem modelling of global total atmospheric Hg depositions

We employed the Global Earth Observing System Chemistry model (GEOS-Chem, version 12.6.3, http://geos-chem.org) to generate global total atmospheric Hg deposition fluxes (90°S–90°N, 180°W–180°E, resolution 2°×2.5°) during 1980-2012. The GEOS-Chem model was driven by MERRA2 meteorological data (2°×2.5°) [8], anthropogenic atmospheric mercury emission (0.1°×0.1°), biomass burning emissions (0.25°×0.25°, https://www.globalfiredata.org/), and internal calculation of ocean flux, soil emissions and re-emission[9]. All the input data were calculated at the resolution of 2°×2.5°. Within the framework of GEOS-Chem, the depositions of three distinct Hg species were simulated: gaseous elemental Hg (Hg^0), gaseous oxidized Hg (Hg^{2+}), and particle-bound Hg (Hg^P), encompassing both dry and wet deposition processes. The modelled atmospheric Hg deposition fluxes referenced in this article are the collective Hg deposition, representing the cumulative sum of the three aforementioned forms of Hg species.

The GEOS-Chem simulation of Hg consisted of wet and dry deposition[10]. Wet deposition exists in Hg^{2+} and HgP by means including washout from precipitation (rain and snow) and scavenging in convective updrafts[11]. The modelled ambient Hg concentrations and wet deposition fluxes were validated using ground observations obtained from the Atmospheric Mercury Network (AMNet, https://nadp.slh.wisc.edu/networks/atmospheric-mercury-network/), Mercury Deposition Network (MDN, https://nadp.slh.wisc.edu/networks/mercury-deposition-network/), the Global Mercury Observation System (GMOS)[12] and observations reported in published journal articles (SI Dataset S2). Normalized mean error (eq 2) was adopted for the evaluation of modelling accuracy.

$$Normalized\ mean\ error = \frac{\sum_i |Simulation_i - Observation_i|}{\sum_i Observation_i} \quad \text{eq 2}$$

Dry deposition refers to the Hg removal process by turbulent transfer and uptake at the ground surface and is observed in Hg^{2+}, HgP, and Hg^0. The deposition speed and flux of dry deposition were modelled with a standard resistance-in-series scheme[11,13,14], including aerodynamic resistance, atmospheric boundary layer resistance, leaf stomatal and cuticle resistance, and soil resistance[13,15,16]. Dry deposition flux highly depends on elevation, atmospheric mercury concentrations, ground surface conditions, and meteorological conditions[17-19]. Compared with wet deposition, it is more difficult to validate the modelled dry deposition with ground observations because measuring methods are not standard and consistent[20-22].

The validation of modelled wet deposition and atmospheric concentration of Hg showed normalized mean errors of 51.4% and 16.7%, respectively (SI Fig. S4). Both errors fall within an acceptable range, consistent with other studies that reported wet deposition estimates with mean errors around 50%, with higher errors in high-altitude/latitude areas[23-25]. However, validating the modelled dry deposition is more challenging due to the lack of standardized ground observation methods[20]. See SI Supporting Text 4 for an extensive discourse on modelling result uncertainty. In the absence of more precise alternatives, we prudently adopted the modelled total (wet + dry) deposition fluxes as a surrogate for actual atmospheric deposition fluxes.

2.3 General Additive Model (GAM) analysis

For cores with upper temporal limits of chronology younger than 2012, we extended the respective Hg accumulation data to 2012 using GAM prediction. The model GAM is powerful in prediction based on a relationship between the response variable with the transformed smooth functions of independent variables[26]. We conducted a non-linear correlation analysis on the impacts of environmental, geographic and emission-related factors on Hg fluxes with each of the four types of natural archives

using the gam package in R. The GAM analysis was conducted for each type of natural archive following procedures (a) variable selections, (b) core selections, (c) GAM model fitting, and (d) validations and diagnostic check.

Variable selection. We collected variable data from global open-source databases and peer-reviewed papers compiled in the database (SI Table S4) in 1980-2012, a period overlapped by MERRA-2 [8], EDGAR [27], and the database. A total of eight variables, out of 20, were selected based on two considerations. First, variables should be independent of each other. The inclusion of a variable should not lead to significant multicollinearity between variables, as indicated by Variance Inflation Factors of all variables should be smaller than 5 and as close to 1 (no correlation) as possible[28,29]. Second, the inclusion of a variable should improve the overall goodness of fit of the GAM model, indicated by a reduced Akaike information criterion value.

Core selection for GAM analysis. While the cores in the database were meticulously chosen, they might still contain errors, stemming from the original papers or our selection process. These errors could become apparent when comparing natural archive Hg records to modelled atmospheric total deposition fluxes. To ensure the precision of the input data for the GAM analysis, we excluded cores that meet the following criteria:

1) peat and lake cores whose accumulation fluxes deviated by more than 10-fold from the modelled atmospheric depositions. Such discrepancies may result from either unaccounted deposition mechanisms that were irrelevant to atmospheric depositions in respective papers or uncertainties of modelled atmospheric depositions.
2) cores with likely inaccurately estimated emissions in the EDGAR dataset in the corresponding grids.

All the excluded cores have been noted in Dataset S1 along with their exclusion reasons.

GAM model fitting. We formulated GAM models for each of the four types of natural archives as eq 3-6 and fitted them using Gamma error distribution with a log link, which is suitable for positive-only data[30]. Smooth function (s) of each variable were configured with a default number of smooth functions (k = 10), a smooth class of a cubic spline basis (bs = 'cr'), and the "REML" method. We trained the models with natural archive flux data from 193 cores and the variable data at respective coring locations between 1980-2012. The variables in brackets presented below are self-explanatory, see SI Table S4 for a detailed explanation of individual variables. The GAM models generate the partial effect of each of the predictor variables on the response variable while holding all other predictor variables constant. Partial effect measures the relationship between the predictor and the response, accounting for the potential nonlinearities and interactions with other variables. A partial effect of 0 suggests that there is no association between the predictor and the response. Values larger/smaller than 0 indicate increasing positive/negative effects.

$$Hg\_Ice \sim s(Elevation) + s(Precipitation) + s(Temperature) + s(Greenness) + s(Global\_TotEmit) + s(Local\_AntEmit) + s(Local\_nonAntEmit) \quad \text{eq 3}$$

$$Hg\_LakeSed \sim s(Elevation) + s(Precipitation) + s(Temperature) + s(Greenness) + s(Global\_TotEmit) + s(Local\_AntEmit) + s(Local\_nonAntEmit) + s(CatchmentArea/LakeArea) \quad \text{eq 4}$$

$$Hg\_Peat \sim s(Elevation) + s(Precipitation) + s(Temperature) + s(Greenness) + s(Global\_TotEmit) + s(Local\_AntEmit) + s(Local\_nonAntEmit) \quad \text{eq 5}$$

$$Hg\_MarineSed \sim s(Depth) + s(Precipitation) + s(Temperature) + s(Greenness) + s(Global\_TotEmit) + s(Local\_AntEmit) + s(Local\_nonAntEmit) \quad \text{eq 6}$$

GAM model validation. The GAM models were validated by checking 1) if the explained deviance is at an acceptable level (normally > 50%); 2) if model fitted value versus core values are close to 1; 3) if the histogram of residuals is close to normal distribution; and 4) if a Q-Q plot with quantiles points closely lie on the 1:1 reference line. If passed validation, the model generated partial effects of each of the eight variables on the respective natural archive Hg records were accepted.

The GAM models were also subjected to 10-fold cross-validation, and the results were presented in SI Table S5. In 10-fold cross-validation, each dataset was randomly divided into ten equally sized subsets (folds). Each model was trained on nine of the folds and validated on the remaining fold. This process is repeated ten times, each time using a different fold as the validation set [31]. The performance metrics from each iteration were averaged to provide an overall evaluation of the model's performance, indicated by the scale parameter of the GAM model (GAMscale) and Mean Squared Error (CV-mse-GAM). GAMscale represents the dispersion or variability of the residuals (errors) in the model, thus the lower the GAMscale value the better. Similarly, a lower CV-mse-GAM value indicates the model's prediction is closer to the true values on average during cross-validation. Especially, the same value of GAMscale and CV-mse-GAM indicates the GAM model is well-fitted with an appropriate level of complexity to capture the relationships between predictors and the outcome variable[32].

GAM prediction. We fed the satisfied GAM models (eq 3-6) with the eight independent variable datasets at coring locations spanning the period 1980-2012, and the models thus provided predicted Hg fluxes over the same period. Based on the available core Hg flux data in each core, we quantified the deviation of the respective predicted Hg fluxes. Only when the mean deviance of the predicted fluxes fell within the one-fold range of the core fluxes, the predicted flux data would be allocated to the years of missing data for that core. In cases where the conditions were not met, the predicted values were considered unreliable, and the core fluxes were thus not extended.

GAM spatial-temporal analysis. We also conducted spatial-temporal GAM analysis by analysing partial effects of year and location on natural archive Hg records at the global scale (221 cores) and regional scale covering Europe, North America and the Arctic (152 cores) during 1980-2012. The spatial-temporal GAM analysis used a smooth term (*f*) with a tensor product of the year and coordinates (eq 7)[33].

$$Hg\_CoreFluxes \sim f(Year, latitude, longitude) \quad \text{eq 7}$$

The GAM result of spatial-temporal analysis for changes in natural archive Hg records was validated by comparing the characterized trends from the regional plots with relevant trends from published independent research. The validation was also performed by comparing the partial effect results in the regional plots with those in global plots (SI Fig. S17). An agreement also indicates good stability and representation of the spatial-temporal analysis.

2.4 Synthesised regional fluxes

The regional Hg fluxes were computed by averaging the Hg flux data, either natural archive records or modelled total atmospheric deposition, in the same region each year. The respective 95% confidence intervals were also determined. For the natural archive Hg records, the synthesised regional Hg accumulation fluxes during 1700-1980 were calculated solely using data from cores. For the fluxes during 1980-2012, both core data and GAM predictions were used to estimate the mean flux and

confidence intervals. The inclusion of GAM predictions is because the number of available cores post-1980 reduced significantly, which may lead to wrong estimates and erroneous conclusions.

2.5 Disparities in magnitude, trends, and changing rate between natural archive Hg records and modelled atmospheric deposition

We quantified the disparities (δ) between core-based natural archive Hg records (f_{core}) and the modelled total atmospheric Hg deposition fluxes in the corresponding grids of the coring locations ($f_{modeled}$) based on eq 8.

$$\delta = \frac{(f_{core} - f_{modeled})}{f_{modeled}} \times 100\% \quad \text{eq 8}$$

The changing rate and trend were determined based on linear regression of data points over the selected periods. The significance of the trend was estimated by Mann-Kendall Test, which is a statistical assessment of existing monotonic upward or downward trends[34], using the Kendall package in R. We used a two-sided p-value lower than 0.05 to reject null hypotheses of no monotonic trend.

Text 3. Natural and anthropogenic impacts on mercury accumulation in natural archives

3.1 Emission-related impacts

Local anthropogenic emissions exerted the foremost influence on lake-Hg and peat-Hg fluxes, evident from the highest F value, indicating the weight of an impact factor. The emissions also significantly influenced marine-Hg fluxes, indicated by the second-highest F value. The implications of changing local anthropogenic emissions on individual sedimentary Hg fluxes were depicted in the partial effect plots presented in SI Fig. S7-14. The partial effect shows the relative change in sedimentary Hg flux levels with variations in the targeted impact factor while keeping other impact factors constant (*ceteris paribus*). These plots show general positive partial effects of local anthropogenic emissions on peat-Hg, lake-Hg, and marine-Hg fluxes, implying that higher local anthropogenic emissions corresponded to increased Hg accumulation fluxes in peat, lake, and marine sediments.

Additionally, local non-anthropogenic emissions exhibited a moderate yet statistically significant influence on lake-Hg, peat-Hg, and ice-Hg fluxes. However, the nature of these partial impacts could be either positive or negative, lacking a consistent directional pattern (see SI Fig. S7,9,11). This fluctuation is likely attributed to the diverse composition of non-anthropogenic emissions, including direct emissions and re-emissions stemming from soil, vegetation, geogenic activities, and biomass-burning activities.

Global total emissions can also significantly affect ice-Hg and peat-Hg fluxes. Notably, after 1990, when global Hg total emissions exceeded 6000 tons/year, the higher emissions led to lower peat-Hg fluxes (SI Fig. 7). However, this negative correlation is an artefact resulting from uneven distribution of peat cores worldwide. A substantial 56% of peat cores in the database were in Europe, a region with decreasing total Hg emissions since the 1950s[35,36]; the increasing global emissions were contributed from other regions, e.g., in East Asia, which potentially have limited direct impacts on peat-Hg fluxes in Europe. This disparity emphasized the importance of carefully considering core distribution when interpreting sedimentary Hg fluxes. Therefore, we confine the discussion of peat-Hg fluxes only in Europe in the upcoming section of spatial-temporal analysis to avoid uncertainties introduced by uneven core distribution.

3.2 Surface temperature impacts

The annual average surface temperatures recorded at the coring locations spanned a range from -54°C to 28°C. SI Fig. S11 shows an increasing positive partial effect, i.e., higher ice-Hg fluxes, as temperatures decreased from -20°C downwards. This increase in fluxes under colder conditions could be attributed to the heightened ice stability because lower temperatures contribute to reduced sublimation[37] and a decreased likelihood of melting during summertime, thereby minimizing the loss of accumulated Hg. Furthermore, at lower temperatures, Hg may be "cold-trapped" and accumulated due to elevated levels of Hg condensation and fractionation from the atmosphere[38].

For marine cores, the GAM result generally shows a negative correlation between temperature and marine-Hg fluxes. Notably, ice melting in the marine environment might have great impacts on marine-Hg fluxes, as eliminates physical barriers and enables the evasion of water-saturated Hg from oceans[39]. Multiple factors at the coastal environment could change marine-Hg fluxes. For instance, 1) melting glaciers and permafrost, as in Greenland[40,41], could transport sediment-bound Hg to continental shelves[42]. 2) Elevated temperatures may modify coastal land cover and increase wildfires[43], enhancing natural Hg emissions and atmospheric deposition. 3) Rising temperatures may increase coastal ecosystem productivity[44], providing greater input of organic matter that bounds Hg[45].

In the terrestrial environment, we found a general positive lake-temperature correlation when temperature above 0 °C, which is likely because warmer temperatures enable the growth of broadleaf plants that actively uptake ambient Hg[46] in catchments, amplifying organic matter-bound Hg supply[45]. Such vegetation impact was measured in GAM by greenness fraction, revealing the third most substantial impact on lake-Hg fluxes following temperature as the second. Moreover, the vegetation impact on lake-Hg fluxes could be further heightened by larger catchments[47,48], a pattern supported by GAM result demonstrating elevated lake-Hg fluxes with larger catchment-to-lake area ratios (≥ 25) (SI Fig. S9). Akin to marine-Hg fluxes, elevated temperatures could stimulate lake primary production, contributing organic matter-bound Hg to lake sediments[49,50]; however, such a relationship is not universally observed[5,51]. Last but not least, meltwater from retreated glaciers has introduced additional Hg inputs aside from atmospheric deposition into the proglacial lakes, mostly in high mountain and polar regions[52-54].

The positive correlation between peat-Hg fluxes and temperatures > ca. 7°C is likely a result of a heightened organic matter-bound Hg input from vegetation growth similar to that happened in lake-Hg fluxes, which outran the simultaneously enhanced microbial activity that decomposes peat[55,56]. Hence, more Hg was retained. Besides, elevated temperatures potentially shorten the duration of the annual freezing period and the depth of frozen peat. Consequently, a greater proportion of Hg is retained within the peat, rather than being expelled alongside pore water during frost exclusion[57]. Moreover, the elevated temperatures are likely to diminish the surface humidity levels of peat, thereby suppressing the generation of water-soluble methylmercury. Therefore, more Hg was retained within the peat, as opposed to its depletion through outflows as methylmercury[58,59].

3.3 Depth/elevation impacts

The bathymetric depths or topographic elevations at coring locations ranged from -960 masl to 5750 masl, and emerged as a paramount factor influencing ice-Hg and marine-Hg fluxes, while also significantly impacting peat-Hg and lake-Hg fluxes (SI Fig. S7 and S9). For bathymetric depths of marine cores, a positive correlation was observed at depths from -100 masl to 0 masl, i.e., the shallower depths, the higher marine-Hg fluxes, possibly indicative of coastal non-atmospheric inputs such as

shore area erosion. Conversely, a negative correlation, i.e., the deeper depths, the higher marine-Hg fluxes, were observed at depths below -300 masl, which may result from sediment focusing[60] and/or sediment export to the deep sea[61,62]. Besides, the ocean serves as a reservoir of historic anthropogenic Hg emissions, with two-thirds stored in water shallower than -1000 masl[63], and Hg concentrations in ocean water columns generally increase with depth, although not always monotonically[62,63]. Such elevated Hg inventories and concentrations at deeper areas of coastal regions could also increase marine-Hg fluxes at deeper depths.

At higher altitudes, topographic elevations influence Hg accumulation in natural archives not only through inherent deposition mechanisms but also by the supply of atmospheric Hg deposition. Primarily, reduced availability of total Hg deposition at high-altitude natural archives might arise due to a significant drop in ambient Hg concentrations beyond the planetary boundary layer at moderate altitudes of 2000-3000 masl[64]. However, a heightened supply of water-soluble Hg^{2+} could be anticipated at high altitudes, converted from Hg^0 owing to increased available free radicals and oxidants, such as bromine and ozone[38,65,66]. Moreover, high-elevation areas of the Tibetan Plateau were found with a gradually amplified warming peaking at around 5000 masl due to climate change[67,68]. This warming may affect land covers especially the ice/snow-covered areas[69,70] potentially altering Hg supplies to lake cores. As an amalgamated effect, we found a generally positive partial effect of elevations on ice-Hg fluxes, but this positive partial effect gradually diminished beyond ca. 4000 masl. Concurrently, a reducing negative partial effect of elevations on lake-Hg fluxes was also observed beyond this threshold. Eventually, the negative partial effect of elevations on lake-Hg fluxes gradually transitioned to a positive partial effect at higher elevations > 4000 masl. These relationships underscore the plausible risks of Hg pollution in high-altitude ecosystems.

Text 4. Uncertainty analyses

4.1 Bias induced by core count and distribution

We acknowledge that this study is subject to unavoidable limitations, primarily stemming from insufficient natural archive records in certain regions. Cores extracted from East Asia, Southeast Asia, South America, and Antarctica are notably scarce. Synthesised regional fluxes derived from fewer cores (< 5) typically exhibit higher uncertainties, as reflected in generally wider confidence intervals in manuscript Figure 3. Additionally, the distances between core locations and emission sources significantly influence natural archive records. For instance, East Asia, with only five lake cores and two peat cores, displays conflicting trends after 1970. This discrepancy arises because the peat cores are not in the same region as the lake cores, and the low number of peat cores compromises the reliability of trends representing peat contamination levels in East Asia. In fact, East Asia shows increasing anthropogenic Hg emissions in EDGAR and elevated atmospheric Hg depositions in GEOS-Chem models from 1980 to 2012 (refer to SI Fig. S15), likely to enhance the Hg accumulations in lake and peat ecosystems.

To mitigate the chances of misinterpretation, our manuscript primarily discusses synthesised fluxes derived from relatively larger numbers of cores (≥ 5) and those derived from fewer cores but with narrow confidence intervals. Due to these considerations, we refrain from presenting synthesised results for Southeast Asia and Antarctica (both having only two cores with large confidence intervals). Nevertheless, the raw flux data of individual cores and synthesised regional fluxes are available in Dataset S1 and S3.

Moreover, no cores were extracted from key countries such as India, Indonesia, and Brazil, which are significant global Hg emission sources, particularly from coal burning and/or artisanal and small-scale

gold mining (ASGM)[71,72]. Therefore, more targeted paleo studies are needed to address these data gaps in the future. Such studies would be valuable for understanding pollution status and facilitating the evaluation of policy effectiveness. The representativeness of the synthesised regional Hg fluxes in the aforementioned areas requires further validation and updates with new data in future studies.

4.2 Uncertainties induced by deposition mechanisms of natural archives

The four types of natural archives exhibit distinct physiochemical mechanisms that can lead to the loss or aggregation of Hg within these archives. We have summarized the impact factors contributing to differences between natural archive Hg records and atmospheric Hg deposition, categorizing these impacts into two phases: before (pre-deposition) and after (post-deposition) Hg reaches and is preserved in natural archives (details see SI Table S1 below). For more comprehensive reviews, see[1,5,73].

As a result, not all natural archive data are comparable or suitable for inferring atmospheric deposition. To enable such comparisons, we conducted careful core selection, focusing on cores proven to be primarily affected by atmospheric deposition (refer to the SI supporting Text 2). Additionally, we further avoided dilution or enrichment of Hg in natural archives due to varying sediment densities and accumulation rates by using data of flux (mg-Hg/m^2/yr) instead of concentration (mg-Hg/kg-sediment).

Certain factors remained unavoidable by simple means of core selection or concentration-to-flux conversion; hence, they were addressed either quantitatively (utilizing GAM results) or qualitatively and discussed in detail in the main text. Note that the same impact factor might have varying effects on different cores of the same type, and each core possesses unique conditions and is subject to different kinds of impact factors.

4.3 Uncertainties induced by chronologies of natural archives

This study analysed 221 cores from 70 individual papers, with the earliest publication dating back to 1989. Given the extensive number of sources, spanning several decades, cross-checking or validating chronological data proved challenging, unlike the scrutiny applied to flux data, where magnitudes were compared among cores from the same regions or coring locations.

In reality, all the determined chronologies bear uncertainties, and sometimes errors, and the dating methods adopted across studies were not uniform. Different methods can yield chronologies with variations of up to 100 years[74,75]. Discrepancies may arise from various factors, including sample collection and handling[73], dating techniques (such as ^{210}Pb, ^{14}C, and counting stratigraphical layers), calibration with independent information (such as nuclear fallout of ^{137}Cs, ^{226}Ra, ^{3}H and ^{239}Pu, tephra layers, and nearby tree-rings). Besides, in multi-core studies, only a limited number of primary cores are dated using instruments, while others are dated using wiggle-matching based on tie points like flux peaks, introducing potentially larger uncertainties.

Furthermore, for this study, linear interpolation was employed between dated sediment layers to obtain annual data. Despite the effort of core selection to constrain the temporal resolution of cores to be finer than 20 years, which is the approximated range of dating errors for ^{210}Pb [6] and ^{14}C[7], such linear interpolation may still introduce chronological errors. Therefore, the natural-archive fluxes discussed in this study are not tied to an exact year but rather to a period of approximately ±10 years.

4.4 Uncertainties induced by concentration-to-flux conversion

Sixteen percent of the total cores, primarily ice and marine cores, underwent concentration-to-flux conversion using constant sedimentation rates. However, sedimentation rates are seldom constant over

time, and typically, more recent periods exhibit higher sedimentation rates than older ones. Consequently, the Hg accumulation fluxes in modern times may be underestimated, and those in the pre-industrial period may be overestimated. Therefore, the flux results should be considered as a lower (or upper) bound.

4.5 Uncertainties of modelled fluxes of total atmospheric Hg depositions

As mentioned in the manuscript, the modelling validation results showed that the normalized mean errors of the modelled wet deposition and modelled atmospheric Hg concentration were 51.4% and 16.7%, respectively (SI Fig. S4); both are at acceptable levels. The modelled wet deposition result shows a general overestimation (underestimation) below (above) ca. 4 $\mu g/m^2/yr$. Compared with wet deposition, it is more difficult to validate the modelled dry deposition with ground observations because measuring methods are not standard and consistent[20].

The accuracy of modelled atmospheric Hg deposition fluxes could be affected by the following factors including but not limited to 1) under/overestimated emissions in EDGAR, which could affect the accuracy of the modelled deposition fluxes. EDGAR adopted a top-down approach that assigns national emissions to 0.1°×0.1° grid based on proxies like populations and roads[76]. 2) Modelled deposition fluxes at high altitudes may entail larger uncertainties than near ground due to errors in air convection modelling[23]. 3) A total of 20%-40% of atmospheric Hg inputs to lake surfaces may be lost due to evasion as a result of photochemical and biological reductions of water-soluble Hg^{2+} to gaseous Hg^0[77,78]. However, the varying evasion rates were set constant at 20% and lake emissions were not differentiated from river emissions in GEOS-Chem[23], which may overestimate the modelled fluxes. 4) There was unavoidably information loss due to grid averaging in GEOS-chem modelling (2°×2.5°).

The uncertainties in modelling wet and dry deposition could have had an influence on accuracy when utilized as a benchmark for comparison with natural-archive fluxes. However, this impact is likely limited to magnitude comparisons rather than trends or changing rates. Besides, the subsequent impact factor analysis using GAM and spatial-temporal analysis employing synthesised natural-archive Hg fluxes were both conducted independently of the modelling outcomes and thus are free from the modelling uncertainties.

4.6 Uncertainties of atmospheric mercury emissions from metal mining

Several global estimates on Hg emissions[35,79] in the 18th and 19th centuries show an unimodal curve with a peak at the same level as contemporary emissions, largely contributed by silver[80], mercury, and gold mining [35] during the Spanish colonization (1570-1850) and Gold Rush era (1800 onwards). These high historical estimates were strongly rebutted by a general “absence” of peaks in geochemical records[4,81,82]. The mean accumulation flux of these geochemical records was further used as a reference to revise the mining emission level to 1/3 of the original[82]. A recently published estimation of the mining emissions[83] was ca. 2/5 to 1/2 of those from Streets et al.[35,84]. Our synthesised regional fluxes largely agree with those findings that mining emissions are likely overestimated and/or only of local impact at large. However, we observed secondary peaks in 12% of cores (26 /221 cores) in the database (Dataset S1) that potentially linked to the proclaimed high Hg emissions. Therefore, we want to draw attention to the use of natural archive records for such validation. If the distances between natural-archive cores and mining locations are beyond the local impact range (from 50 km[85] to 100 km[86]), the natural-archive fluxes might be biased in evaluating and calibrating mining emissions. No cores from California, USA, the hotbed of the Gold Rush, were analysed by Zhang et al.,[82] and Engstrom et al.,[4] (neither were in this study). Let alone natural-archive fluxes are also affected by

various pre- and post-depositional processes as proved in previous modelling and GAM analysis. For instance, the lake-Hg or peat-Hg fluxes typically surpassed respective atmospheric total depositions, potentially leading to an overestimation of adjusted emissions if they were used as references. Employing natural archive fluxes as validation or calibration references for emissions estimates could introduce significant uncertainties or potential errors. Therefore, their use should be approached with caution.

Fast forward to the modern era, ASGM, which retains the use of Hg to extract gold, was believed to top coal combustion and contributed the highest amount of atmospheric Hg emissions (838 tons) in 2015, albeit with large uncertainties (675-1,000 tons)[35,36]. Interestingly, the gold production in South Africa, which used to be the world's largest gold producer, declined from ca. 700 tons/year in 1980 to 121 tons/year in 2017 (SI Fig. S16) with 9.4% contributed by ASGM [72]. Such large gold production was partly contributed by ASGM, either regulated or illegally. South Africa was among the largest exporters of illegally sourced gold in Africa [87,88], although there is no official data disclosing ASGM's contribution to total gold production. If assuming the ASGM gold production changes in parallel with the nation's total gold production, the respective ASGM Hg emissions in South Africa theoretically should also decline no matter estimated with a constant emission factor of losing 75% Hg-used[81] or considering more compliance with environmental regulations that lower the emissions over time. The declining emission trend, however, contradicts the continuous rising accumulation trend revealed by a nearby lake core located in Lesotho[89] (SI Fig. S16), which is under the impact of both coal-fired power plants (the nearest is 200 km away, SI Fig. S17) and ASGM emissions (coring site is inside of the nearest ca. 100 km^2 grid of modelled emissions[81]) in South Africa. Therefore, the demise of the former world's largest gold producer seemed to have little impact on the Hg accumulation ca. 100 km away, which implies a possible overestimation of ASGM emissions and/or such emissions might only be of local impact and a likely more significant impact of coal combustion. More follow-up studies are needed to further validate and eventually narrow the uncertainties of ASGM emissions.

Table S1 A summary of pre- and post-depositional processes of Hg to natural archives contributing to differences between natural archive Hg records and atmospheric Hg deposition. Those process impacts were either avoided, analysed or remained undealt. The treatment of each process was indicated by respective numbers listed in the respective columns.

Natural deposit	Processes with impacts	Impact avoided by core selection	Impact avoided by flux conversion	Impact avoided by adjustment (done by original papers)	Impact analysed in GAM	Remaining impacts
Ice/snow	**Pre-deposition** 1. Hg photochemical reduction (depletion)[90]. 2. Recovery of depleted Hg on ice surface due to sea-ice dynamics and availability of oxidants[91]. 3. Chemical composition of snow and ice, e.g., sea ice contains more chloride that suppresses photoreduction than land ice[92]. **Post deposition** 4. Thawing and percolation of ice and glaciers[93] lead to the loss of the accumulated Hg. 5. Ice and snow density differences due to compression.	4				1 2 3 5
Peat	**Pre-deposition** 1. Anthropogenic/natural disturbances, e.g., peat burning. 2. Peatland types: minerogenic peatland receives Hg from terrestrial water inputs and atmospheric deposition, and ombrotrophic peatland receives Hg only from atmospheric deposition. 3. Morphology of peat: Hummocks and hollows tend to lose and retain Hg[73].	1 2 3 13	6	7 (some)	5	4 8 9 10 11 12

Natural deposit	Processes with impacts	Impact avoided by core selection	Impact avoided by flux conversion	Impact avoided by adjustment (done by original papers)	Impact analysed in GAM	Remaining impacts
	4. Retention by and bioaccumulation in mire vegetations may lead to elevated flux in the surface layers[94,95]. 5. Change of mire vegetations affects Hg concentration levels in peat, generally grassland herbs < trees and shrubs < aquatic macrophytes < Sphagnum < mosses < lichens < fungi[96]. **Post-deposition** 6. High (low) peat bulk density and low (high) permeability lead to peaks (humps) of accumulated Hg[97]. 7. Organic matter accumulates Hg[55,56,98,99]. 8. High humidity levels (net surface moisture) provide anaerobic conditions and enhance methylation, eventually leading to the loss of MeHg from peat[58,59]. 9. Change of hydrological conditions, e.g., extended drought events loss Hg from peatland[100]. 10. High sulfate deposition could change the microbial and chemical environment of peat and eventually reduce the evasion of Hg to the atmosphere[101,102]. 11. Higher microbial decomposition of peat (thinning of peat), due to concurrent oxygenation of deeper peat layer[103], may release preserved heavy metals. 12. Annual freezing and thawing of peat active layer move Hg downwards[57,104]. 13. In diagenetic processes, Hg adheres to and moves with oxides and hydroxides (Fe, Mn) with higher redox potential in peat[73].					

Natural deposit	Processes with impacts	Impact avoided by core selection	Impact avoided by flux conversion	Impact avoided by adjustment (done by original papers)	Impact analysed in GAM	Remaining impacts
Lake sediments	**Pre-deposition** 1. Bio-disturbance, e.g., change in lake ecosystem productivity[49,50,105], and bird excrement provided Hg inputs to lakes[106]. 2. Melting glaciers and ice provide extra Hg inputs[52,93]. 3. A larger ratio between catchment areas and lake areas indicates a larger amount of Hg input from the catchment to lake sediments[107]. 4. Natural or manmade disruption in the catchment, e.g., forest fire and wood clearing in catchment areas. 5. Change of catchment land cover affects Hg fluxes in lakes, e.g., dense forests in catchment increase Hg fluxes in lakes[108]. 6. Catchment legacy Hg input[86,109,110]. 7. Change of Hg input due to change in lake water budget, including surface inflows and outflows and groundwater[94,111]. 8. Lake surface evasion of Hg to the atmosphere[47,77,112]. 9. Elevation affects the supply of atmospheric Hg deposition[65,113]. **Post-deposition** 10. Sediment bulk density. 11. Sediment focusing heightens Hg fluxes in lake sediments[114]. 12. Sediment texture/grain sizes, e.g., clay and fine sizes accumulate more heavy metals.	4 7 15	10	11 (some) 13 (some)	3 5 9	1 2 5 6 8 12 14 16 17 18 19

Natural deposit	Processes with impacts	Impact avoided by core selection	Impact avoided by flux conversion	Impact avoided by adjustment (done by original papers)	Impact analysed in GAM	Remaining impacts
	13. Organic matter content in sediments. 14. Hg dilutions by natural lithogenic components in sediments or erosions from the catchment[65]. 15. In diagenetic processes, Hg adheres to and moves with oxides and hydroxides (Fe, Mn) with higher redox potential in sediments[113]. 16. Oxygen levels of water. Anoxic and suboxic environments lead to reduction conditions, releasing Fe and Mn, as well as the adsorbed metals to the water (Gawel2014). 17. The acidity of lake water, e.g., low pH of water tends to release Hg to the water. 18. Bio-disturbance at water-sediment interface. 19. Lake water level change disrupts sedimentation hence affecting metal accumulation[111].					
Marine sediments	**Pre-deposition** 1. River Hg input[115]. 2. Coastal erosion[42]. 3. Glaciers and permafrost melting[116,117]. 4. Bio-disturbance, e.g., change in marine ecosystem productivity[45]. 5. Air-water Hg exchange, including evasion[45,62,118]. 6. Waterbody stores and buffers Hg deposition[63,82,119]. 7. Water current transport of Hg across regions. **Post-deposition** 8. Sediment bulk density.	1 13	8			2 3 4 5 6 7 9 10 11 12

Natural deposit	Processes with impacts	Impact avoided by core selection	Impact avoided by flux conversion	Impact avoided by adjustment (done by original papers)	Impact analysed in GAM	Remaining impacts
	9. Sediment focusing heightens Hg fluxes in marine sediments[60]. 10. Sediment texture/ size 11. Sediment is exported to the deep sea with the downward flux of aggregates[61,62]. 12. Bio-disturbance at water-sediment interface. 13. Diagenetic processes.					

Table S2 Spatial coverage of natural archive records

Region	Note	Countries/regions with cores	Country/region count	Core count
North America		Canada, USA	2	104
Europe		Czech, Ireland, Norway, Portugal, Spain, Sweden, UK, France	8	24
The Arctic		Greenland, Canada	2	24
Latin America	Central America and South America	Peru, Mexico, Argentina, Chile, Ecuador, Jamaica, Barbuda, El Salvador, Falkland Islands	9	20
Central Asia	Elevation areas (>2000 masl)	China, Nepal	2	17
East Asia	China (≤2000 masl)	China, Japan	2	13
Central and southern Africa		Lesotho, Tanzania, Uganda	3	7
Oceania		New Zealand, Australia	2	5
Southeast Asia		Singapore, Philippines	2	3
Antarctica		Antarctica	1	3
Indian Ocean		Amsterdam	1	1
Grand Total			**34**	**221**

Table S3 Descriptive statistics of mercury accumulation flux in natural archives over three centuries. The number of data is the total data points in each type of natural archive during each period without GAM prediction. The Hg flux data for each year within a core is individually counted as a unique data point.

Type of archive	**1700-1799**			**1800-1899**			**1900-2012**			**1980-2012 (Contemporary)**		
	Number of data	Mean	SD	Number of data	Mean	SD	Number of data	Mean	SD	Number of data	Mean	SD
Lake sediments	5145	0.0090	0.0103	10194	0.0129	0.0209	16119	0.0383	0.0891	3593	0.0548	0.1234
Peat	1094	0.0071	0.0071	1816	0.0144	0.0172	2680	0.0302	0.0323	557	0.0331	0.0344
Ice	382	0.0002	0.0002	500	0.0004	0.0005	659	0.0026	0.0067	212	0.0015	0.0043
Marine sediments	337	0.0145	0.0196	966	0.0290	0.0266	1924	0.0682	0.0889	290	0.1235	0.1745

Table S4 Data sources, process methods, and selection of variables for GAM analysis

Variable type	Factor type	Long name	Used in GAM?	Short name (only for selected ones)	Data description	Data sources	Validation
Independent variables	Geographic factors	Longitude			Longitude of coring location	Literature	
		Latitude			Latitude of coring location	Literature	
		bathymetric depth or Topographic elevation	√	*Depth/Elevation*	Elevation (masl) at lake surface for lake cores. Elevation at the core top for ice and peat cores. Ocean depth (negative masl) for marine cores	Literature SRTM 30 m DEM [120]. We prioritized literature disclosed values over the open-source DEM data.	
		Catchment area vs. lake area	√	*CA/LA*	The ratio between the catchment area and lake area, only for lake cores	Literature SRTM 30 m DEM [120]. We prioritized literature disclosed values than estimated from open-source DEM data	
	Environmental factors	Surface albedo				MERRA-2 2°×2.5°	MERRA-2 data were reanalysis products based on satellite observations and these data were evaluated, validated and updated with ground and aircraft observations [121,122]
		Ice-covered fraction of tile					
		Leaf area index					
		Precipitation	√	*Precipitation*	Annual mean precipitation (mm) at the respective 2°×2.5° grids of coring locations		
		2-meter specific humidity					

Variable type	Factor type	Long name	Used in GAM?	Short name (only for selected ones)	Data description	Data sources	Validation
		Surface velocity scale					
		Temperature	√	*Temperature*	Annual mean air temperature (°C) at 2 meters above ground at the respective 2°×2.5°grids of coring locations		
		Greenness fraction	√	*Greenness*	Annual mean green colour area percentage at the respective 2°×2.5°grids of coring locations		
	Emission related factors	Local anthropogenic emissions	√	*Local_AntEmit*	The sum of the annual anthropogenic elemental Hg, anthropogenic divalent Hg, and anthropogenic particulate Hg at the respective 0.1°×0.1° grids of coring locations (kg).	EDGAR 0.1°×0.1°	The uncertainty of EDGAR Hg emission data derives from various parts, including activity data, emission factors, Hg removal efficiency, and gridding [27,123]. We found that the locations of 13 out of 199 cores in the database were assigned with likely erroneous Hg emissions in EDGAR (See Dataset S1)
		Global anthropogenic emissions					
		Local re-emissions					
		Local total emissions					
		Local non-anthropogenic emissions	√	*Local_nonAntEmit*	The sum of the annual ocean emission, land re-emission, natural land source, biomass burning, vegetation emissions, soil emissions, and snow emissions at the respective	GEOS-Chem output 2°×2.5°	

Variable type	Factor type	Long name	Used in GAM?	Short name (only for selected ones)	Data description	Data sources	Validation
					2°×2.5° grids of coring locations (kg).		
		Global non-anthropogenic emissions					
		Global re-emissions					
		Global total emissions	√	*Global_TotEmit*	The sum of the annual anthropogenic emissions and non-anthropogenic emissions at all grids (ton), except the grids of coring locations.		
Response variables	Natural archive Hg flux	Hg accumulation fluxes in lake sediments	√	*Hg-LakeSed*	All natural-archive data from lake cores except those cores found to have possible erroneous local anthropogenic emissions in EDGAR	The database (this study)	
		Hg accumulation fluxes in marine sediments	√	*Hg-MarineSed*	All natural-archive data from marine cores		
		Hg accumulation fluxes in peatlands	√	*Hg-Peat*	All natural-archive data from peat cores except those found to have possible erroneous local anthropogenic emissions in EDGAR		
		Hg accumulation fluxes in ice cores	√	*Hg-Ice*	All natural-archive data from ice cores, no snow cores included		
		Hg accumulation fluxes in all four types of natural archives in the database	√	*Hg-CoreFlux*	All natural-archive data in the database without excluding any cores.		

Table S5 GAM 10-fold cross-validation analysis. GAMscale refers to the scale parameter of the GAM model; CV-mse-GAM refers to the Mean Squared Error obtained using cross-validation for GAM analysis.

GAM analysis	**GAMscale**	**CV-mse-GAM**
Lake cores	0.0002	0.0002
Peat cores	0.0001	0.0001
Marine cores	0.0000	0.0000
Ice cores	0.0008	0.0012

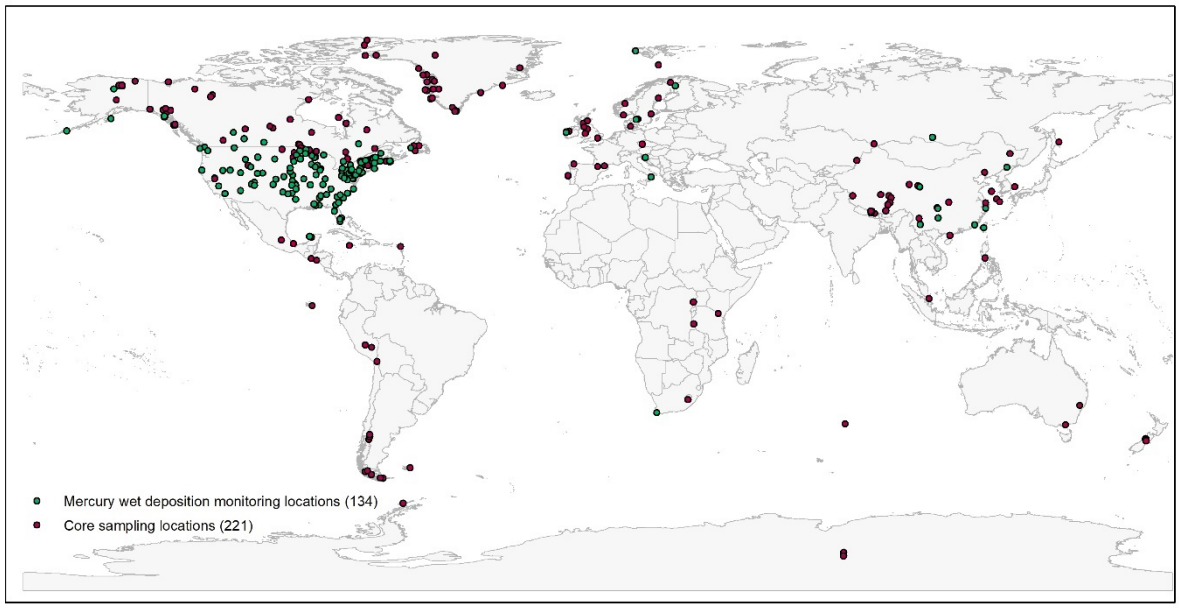

Fig. S1 Spatial distribution of sampling locations of natural archive cores used in this study (SI Dataset S1) and ground monitoring stations of mercury wet deposition (SI Dataset S2).

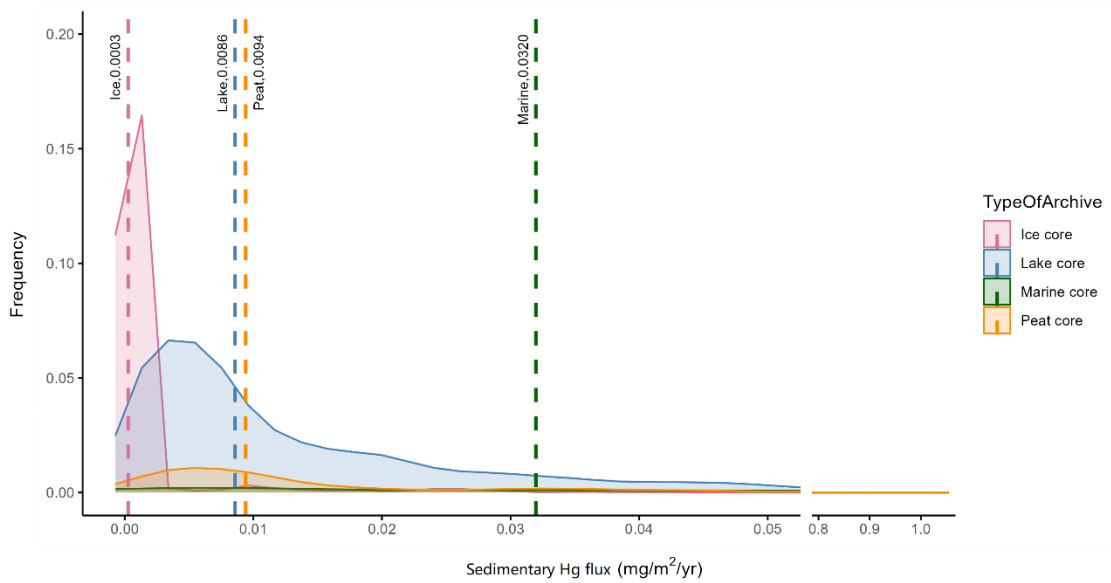

Fig. S2 Data frequency of mercury accumulation fluxes in the four types of natural archive 1700-2012. The dotted lines were median fluxes.

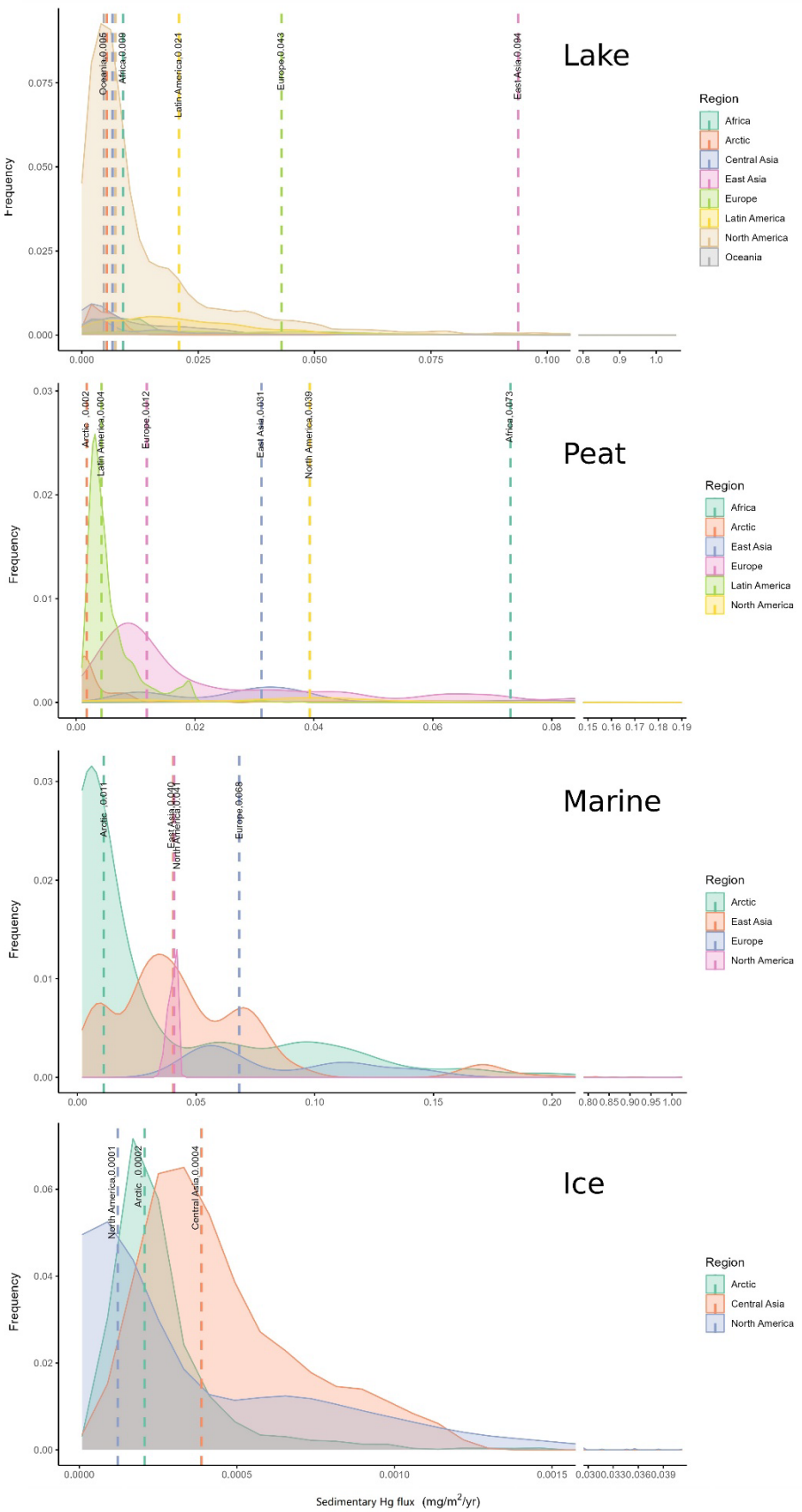

Fig. S3 Data frequency of mercury accumulation fluxes in the four types of natural archive by region 1700-2012. The dotted lines were median fluxes of regions.

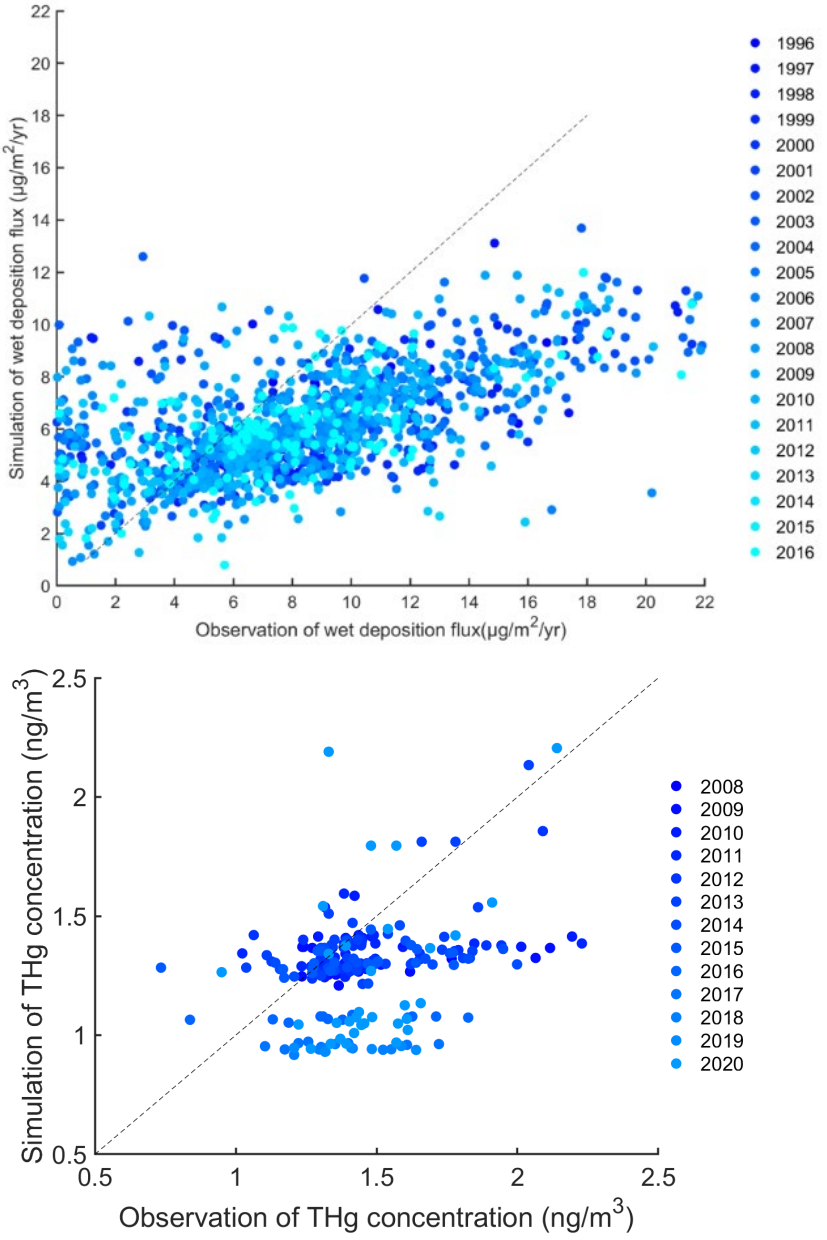

Fig. S4 GEOS-chem modelled wet depositions (upper) and concentrations (lower) vs ground observation of Hg. For wet depositions, the validation shows a deviation of normalized mean bias ($\frac{\sum_i(Simulation_i - Observation_i)}{\sum_i Observation_i}$) of -40.2% and normalized mean error ($\frac{\sum_i |Simulation_i - Observation_i|}{\sum_i Observation_i}$) of 51.4%. The result shows a general overestimation (underestimation) of the modelled wet deposition below (above) ca. 4 μg/m^2/yr. For Hg concentrations, the validation shows a normalized mean bias of -12.4% and a normalized mean error of 16.7%, This validation result shows high consistency between the modelled concentrations with the observed which indicates the robustness of the model.

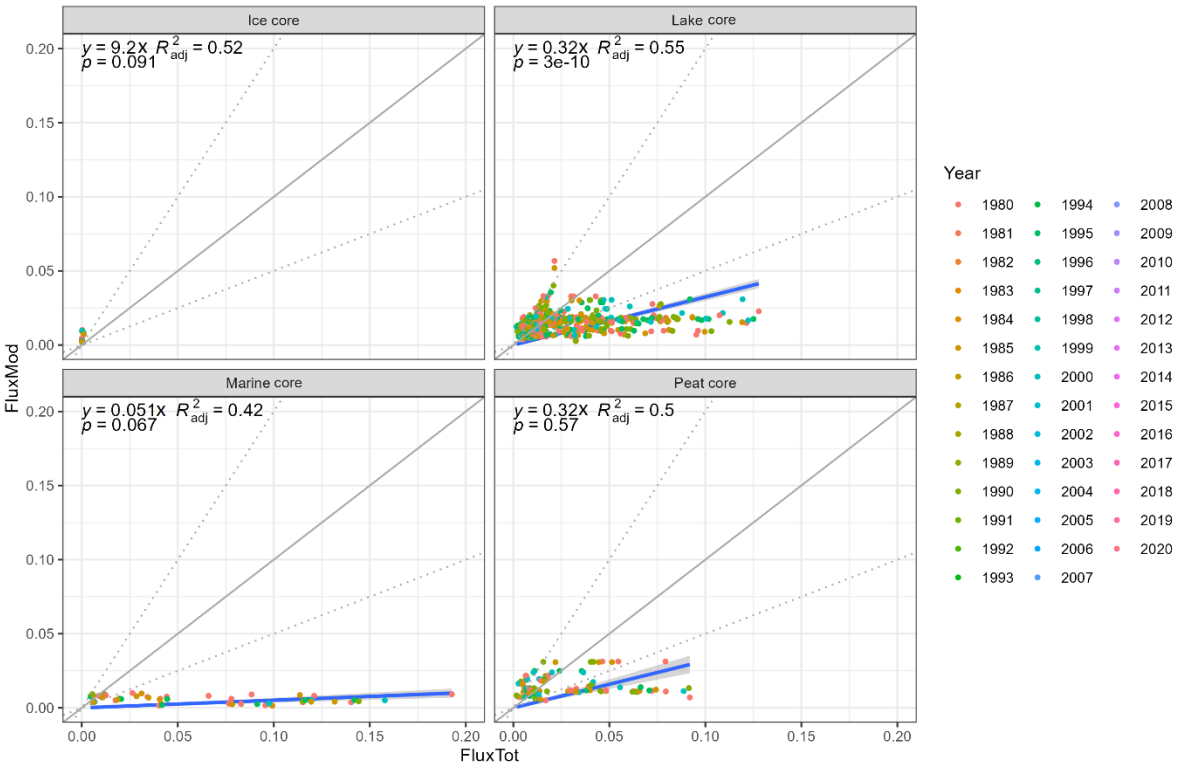

Fig. S5 Natural archive Hg fluxes vs GEOS-chem modelled fluxes using data from 1980 to 2020. The solid grey line is a reference line of y=x, dotted grey lines are y = 2x and y = 1/2x, respectively. Blue lines are fitted regression lines using a no-intercept ordinary linear regression model.

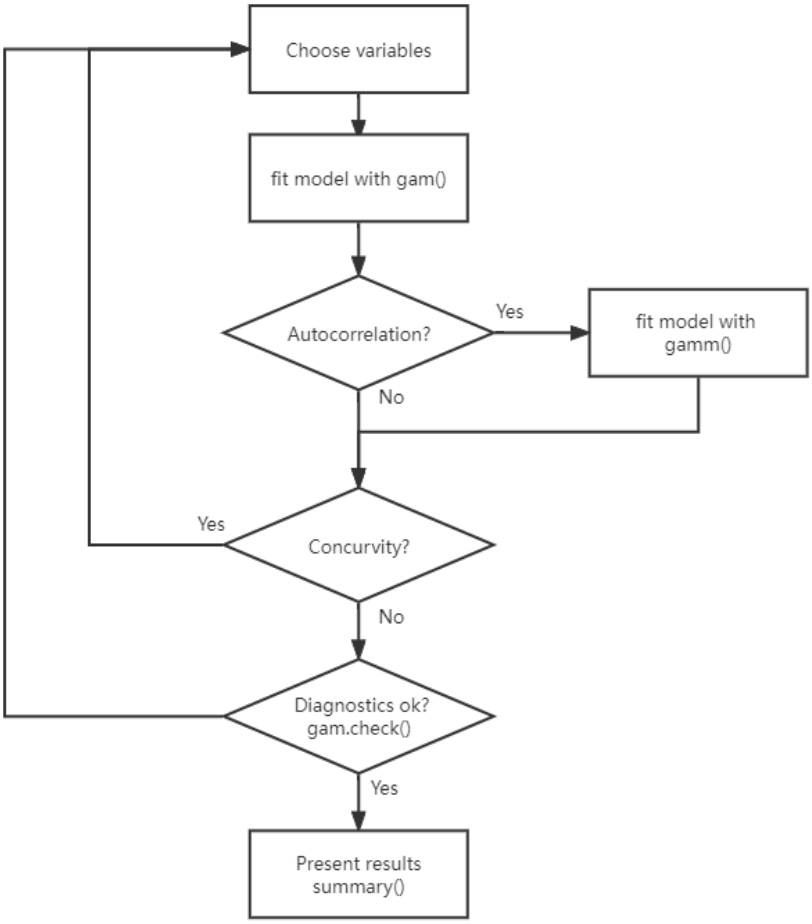

Fig. S6 GAM analysis flow chart

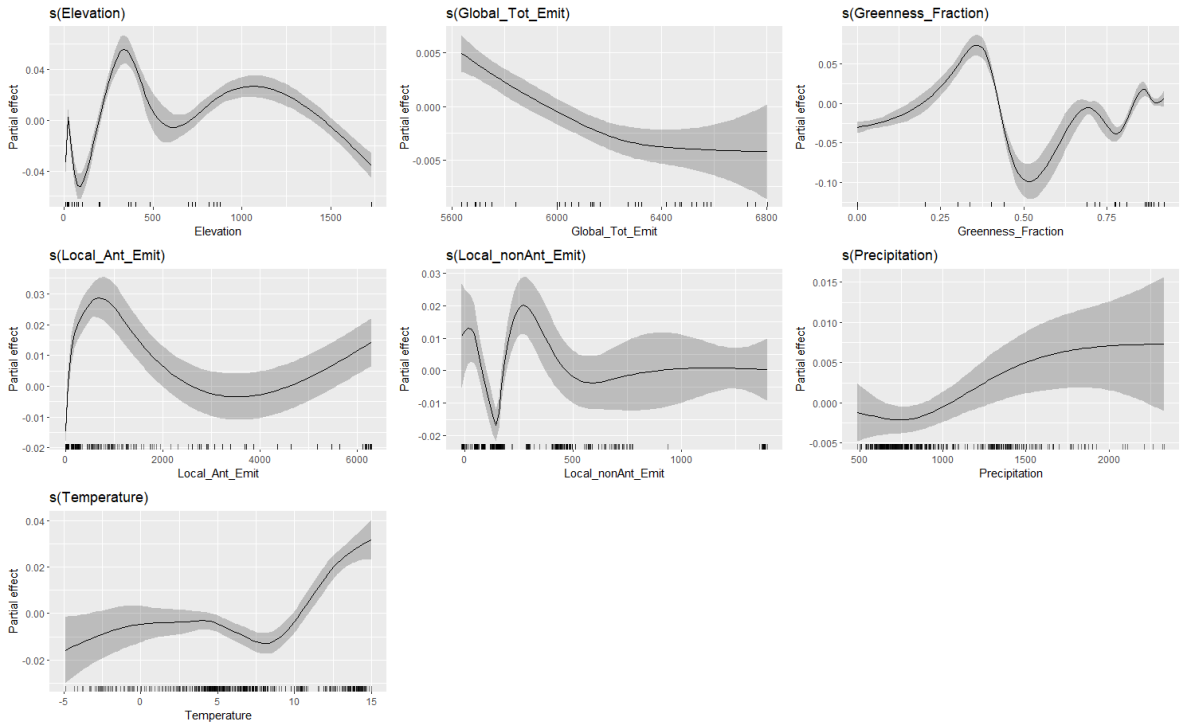

Fig. S7 Partial effects of variables on the natural-archive Hg fluxes from peat cores.

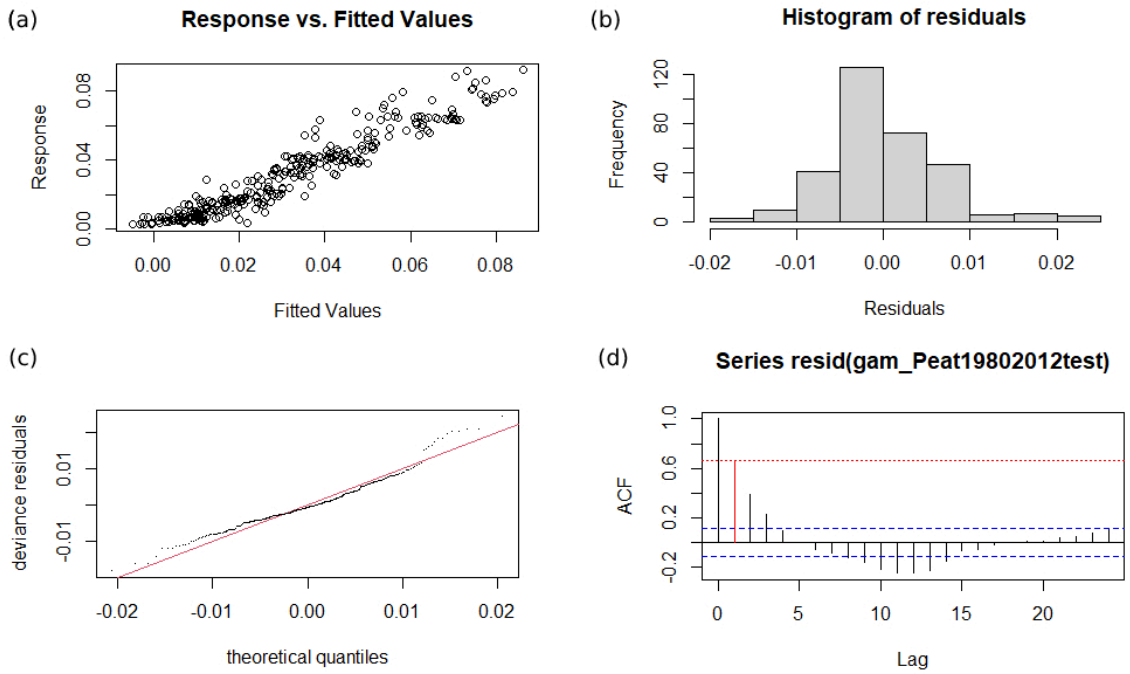

Fig. S8 GAM result check plots for peat cores. (a) fitted value and natural-archive Hg flux values for peat cores. (b) Histogram of residuals of the fitted values for peat cores. (c) QQ plot for GAM fitted results for peat cores. (d) Autocorrelation of simulated residuals for peat cores.

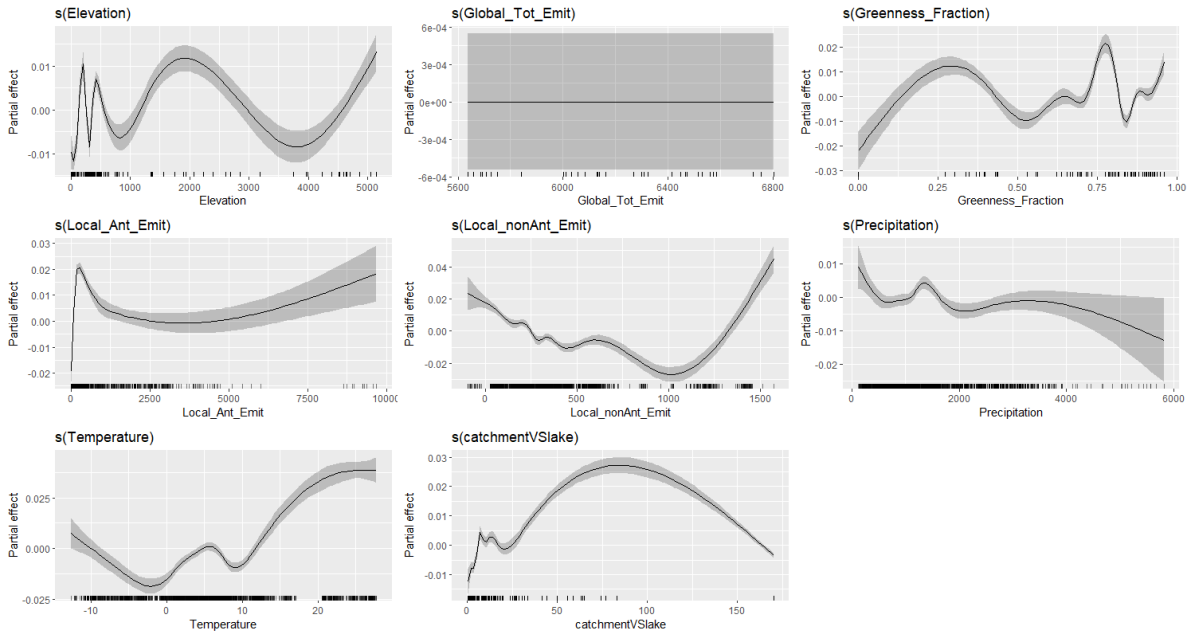

Fig. S9 Partial effects of variables on the natural-archive Hg fluxes from lake cores.

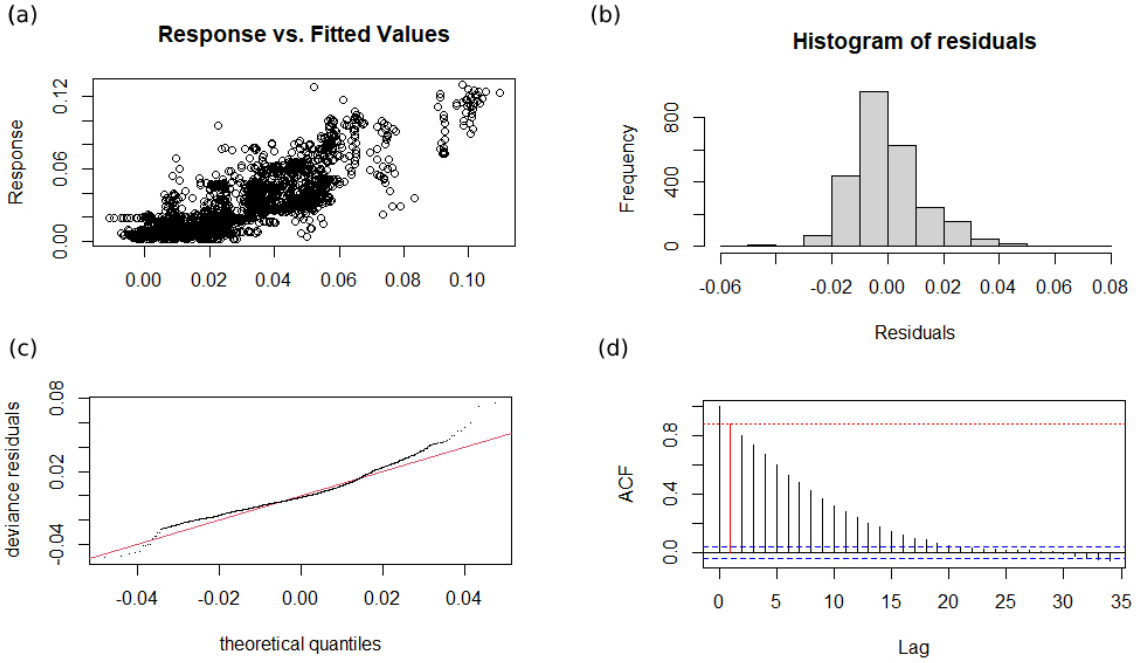

Fig. S10 GAM result check plots for lake cores. (a) fitted value and natural-archive Hg flux values for lake cores. (b) Histogram of residuals of the fitted values for lake cores. (c) QQ plot for GAM fitted results for lake cores. (d) Autocorrelation of simulated residuals for lake cores.

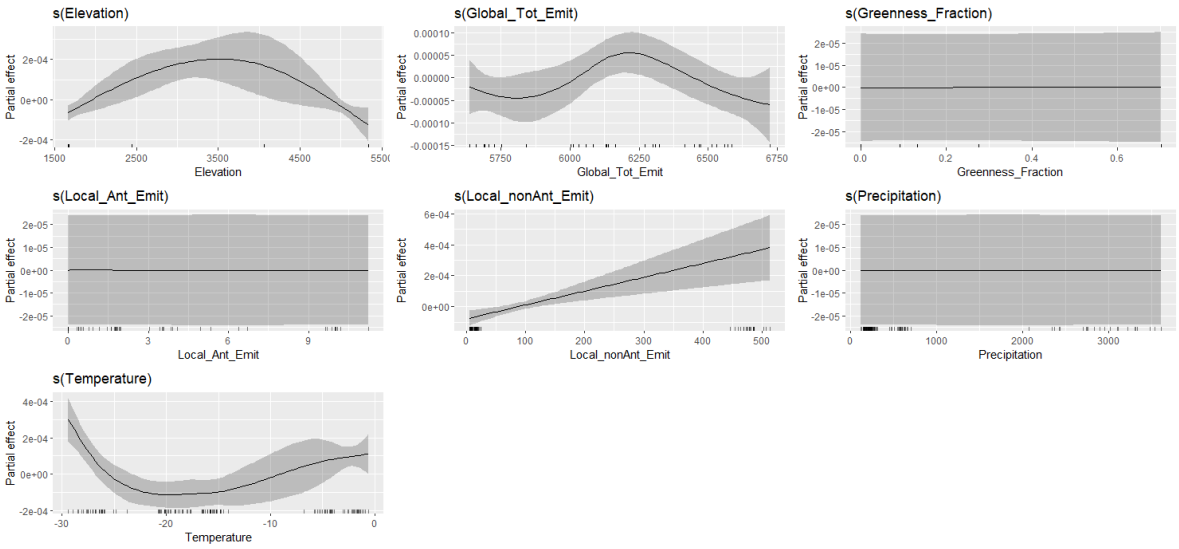

Fig. S11 Partial effects of variables on the natural-archive Hg fluxes from ice cores (excluding snow cores (2 cores)).

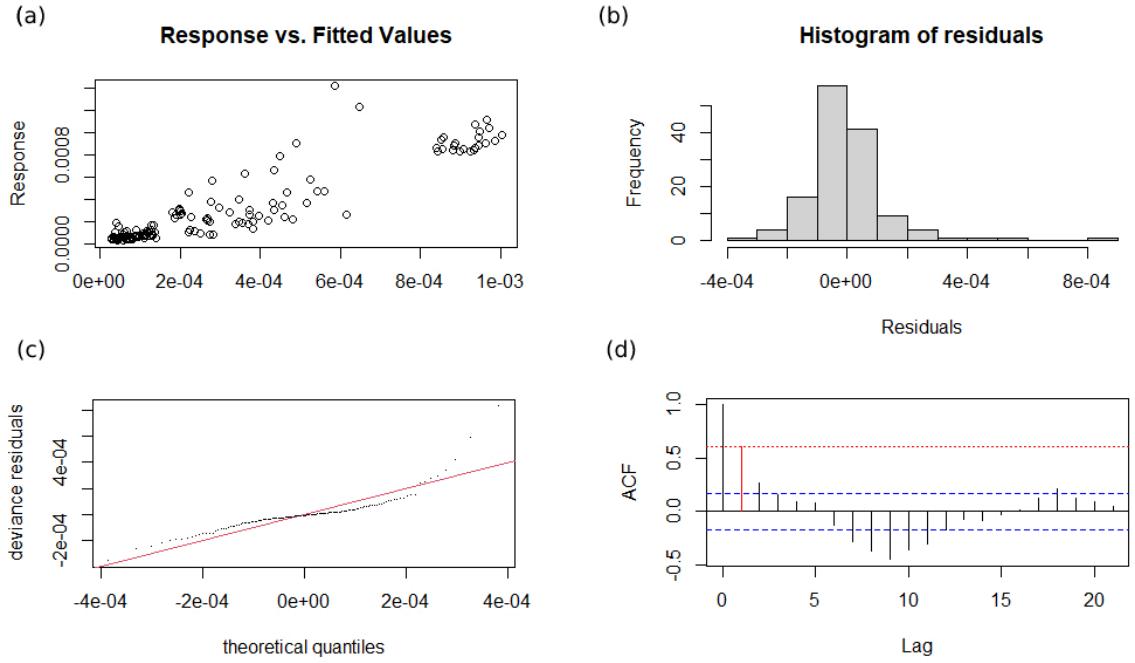

Fig. S12 GAM result check plots for ice cores. (a) fitted value and natural-archive Hg flux values for ice cores. The scattered samples in the central plot are the Greenland ice core [66]. If removing these samples, the GAM model would not converge due to a limited number of ice core samples. Therefore, we keep these samples. (b) Histogram of residuals of the fitted values for ice cores. (c) QQ plot for GAM fitted results for ice cores. (d) Autocorrelation of simulated residuals for ice cores.

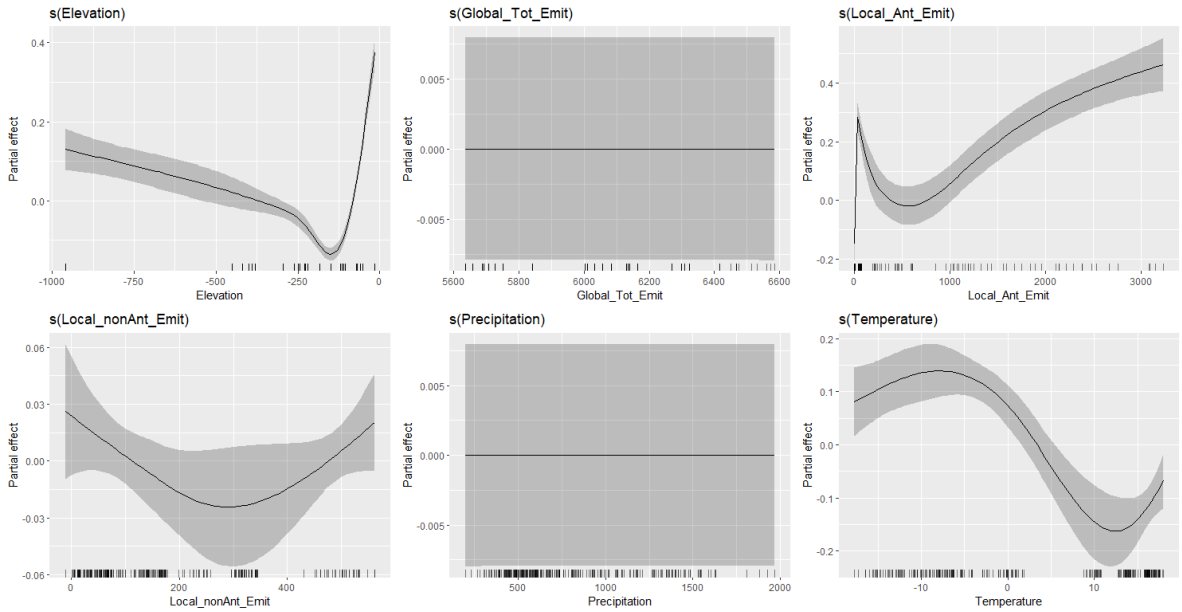

Fig. S13 Partial effects of variables on the natural-archive Hg fluxes from marine cores.

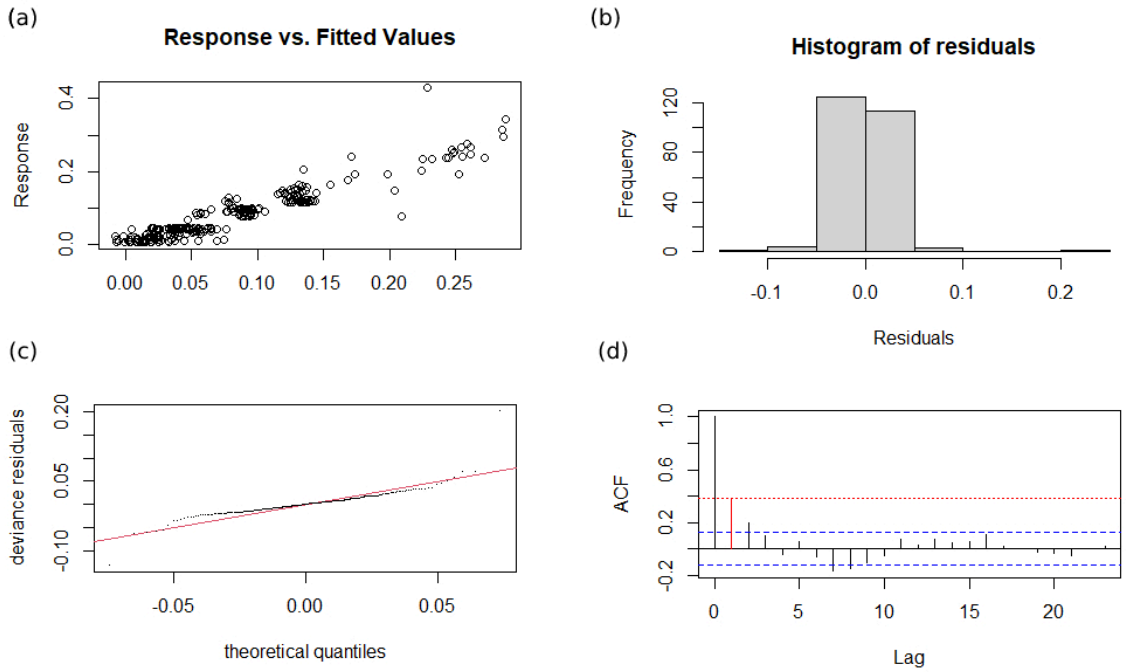

Fig. S14 GAM result check plots for marine cores. (a) fitted value and natural-archive Hg flux values for marine cores. (b) Histogram of residuals of the fitted values for marine cores. (c) QQ plot for GAM fitted results for marine cores. (d) Autocorrelation of simulated residuals for marine cores.

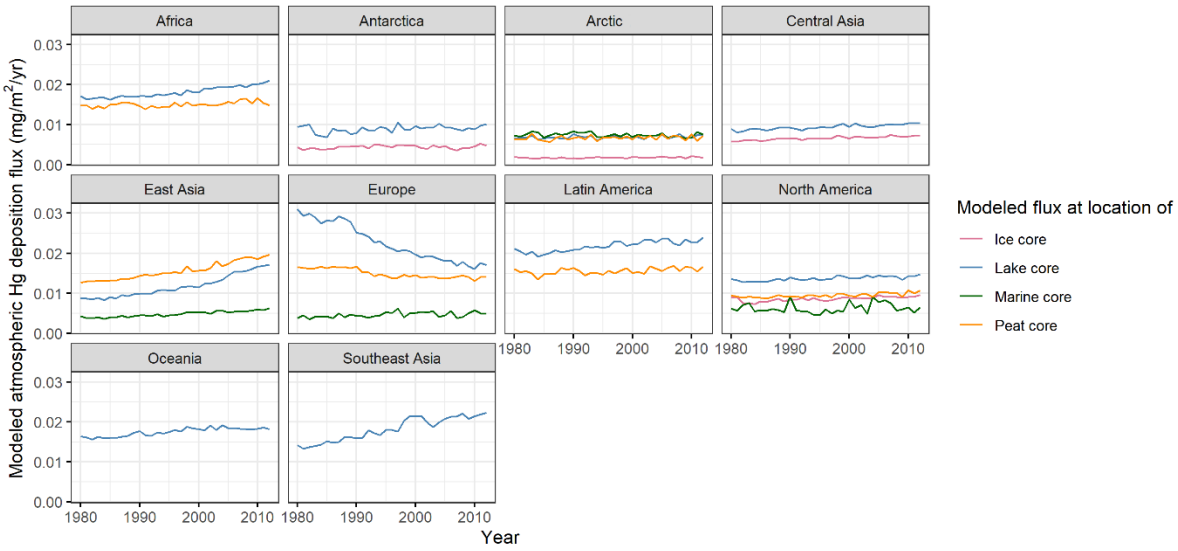

Fig. S15 GEOS-Chem modelled atmospheric Hg deposition at locations of cores by region 1980-2012. Africa refers to Central and Southern Africa, Oceania refers to Australia and New Zealand, Latin America refers to Mexico and the western Andes, and the Arctic refers to Greenland and nearby islands.

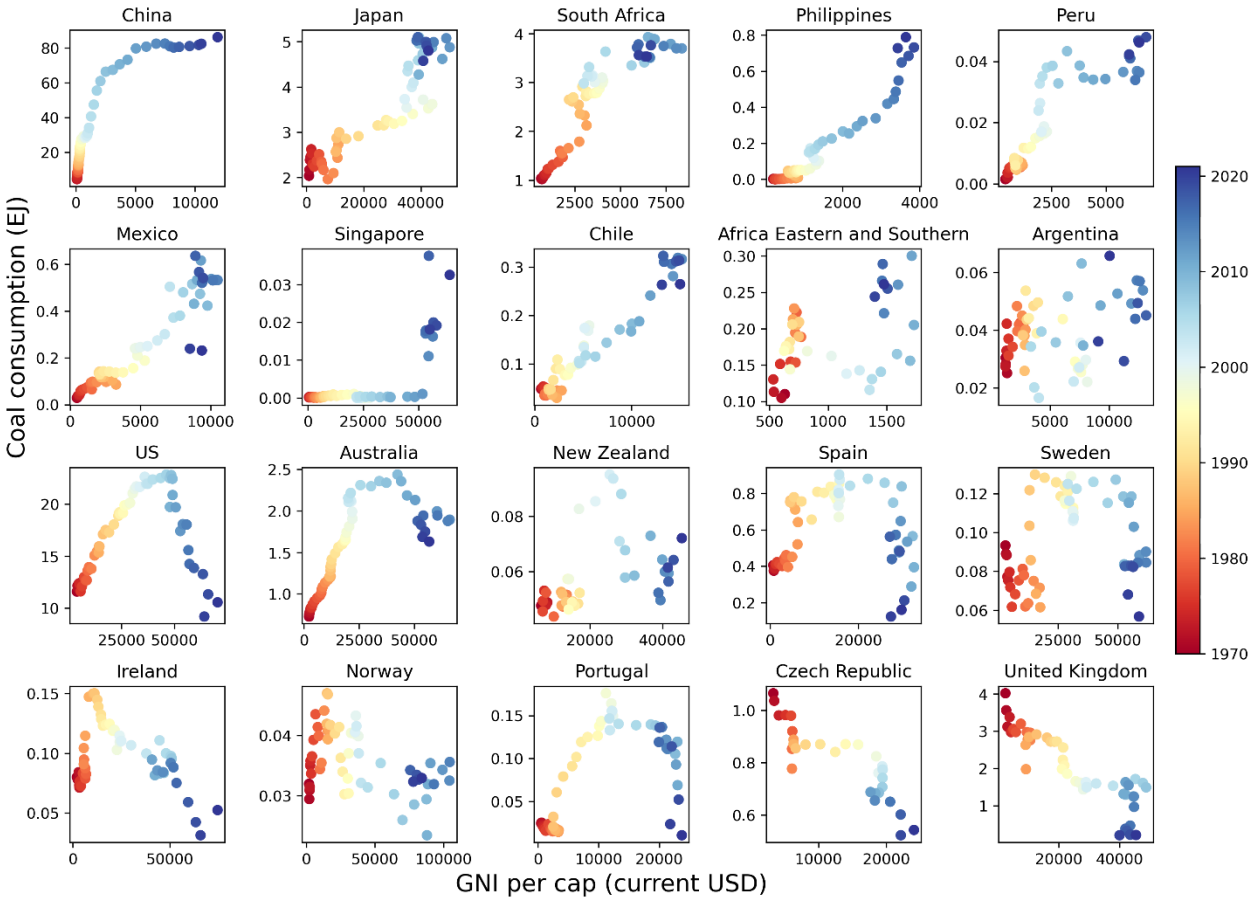

Fig. S16 Scatter plots of coal consumption (EJ) [124] and economic development indicated by GNI per cap (current USD)[125] between 1970 and 2021 in 20 key countries in the database. The simple plots indicate that East Asian countries including China and Japan, African countries including South Africa, and Latin American countries Peru, Mexico, and Chile, have yet to decouple their coal use from economic development. By contrast, North American countries including the US, and European countries including Spain, Sweden, Ireland, Norway, Portugal, Czech, and the United Kingdom, have already decoupled their coal consumption with economic development.

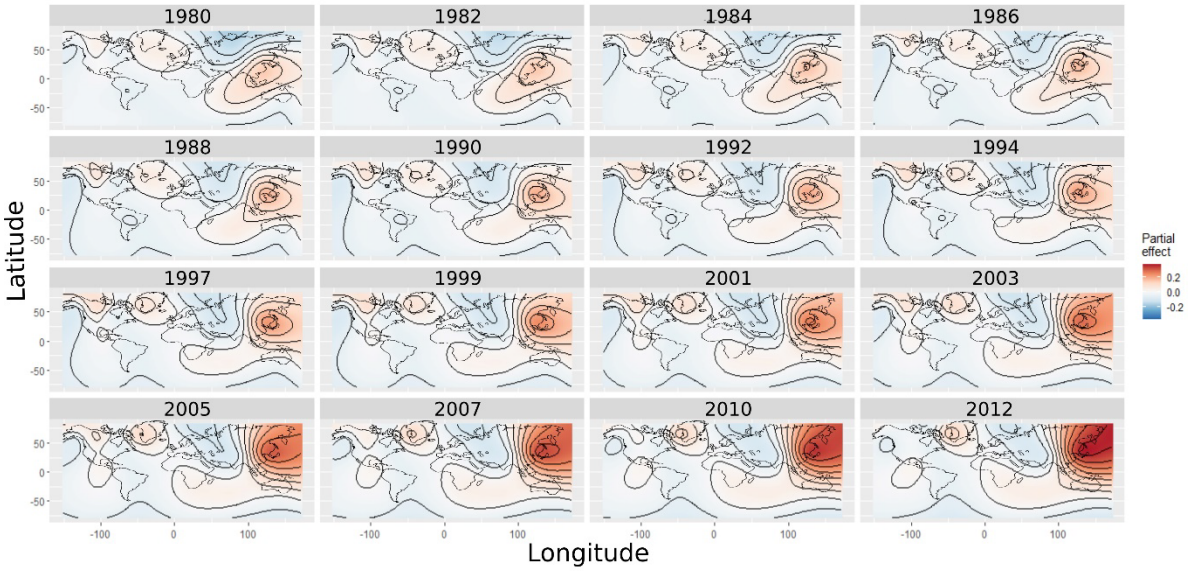

Fig. S 17 GAM partial effect of spatial-temporal analysis across the globe from 1980 to 2012. The findings indicate decreasing accumulation fluxes in North America and Europe, intensified accumulation hotspots in Asia and the Pacific (terrestrial environment), and a newly formed hotspot in the Arctic (marine environment) after 1990. Note that the plotting result may be biased by core types and core distribution.

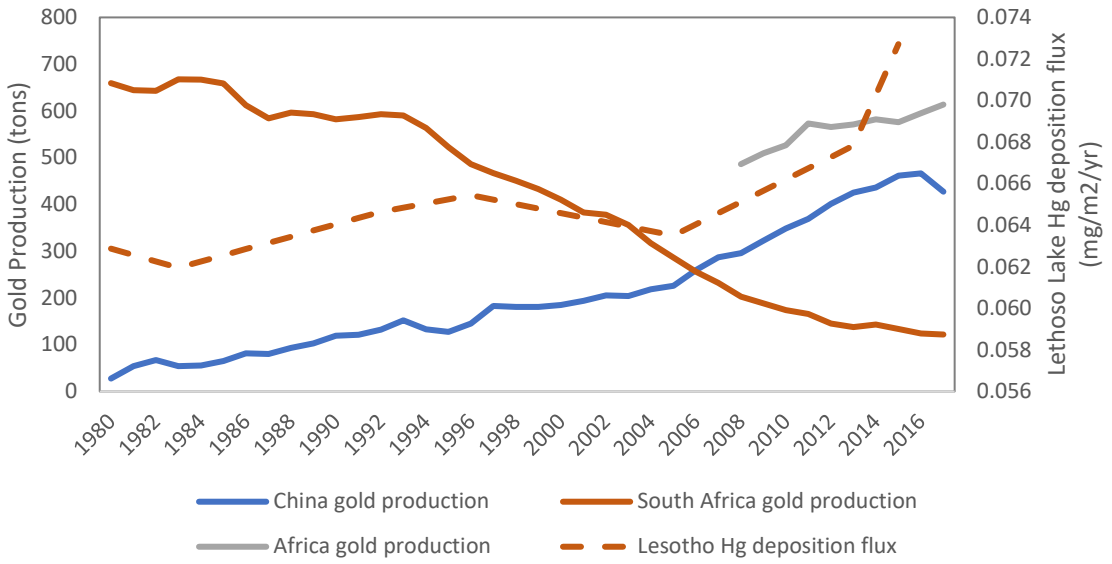

Fig. S18. Gold production in key regions and Lesotho lake Hg accumulation flux 1980-2017. The production in South Africa and China was from Verbrugge et al.[72], and the production in Africa between 2008 and 2017 was from Thomson Reuters [126]. Lesotho lake Hg accumulation flux data were from Rose et al. [127]. Lesotho is a country fully encircled by South Africa.

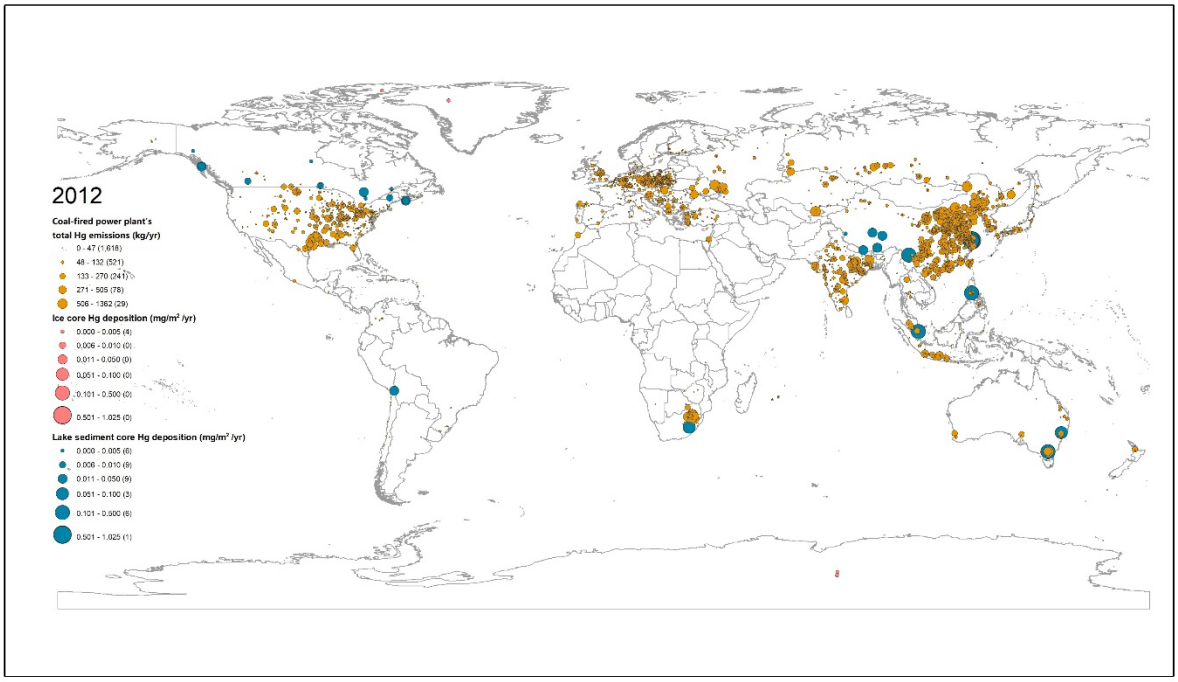

Fig. S19 Natural archive Hg records (mg/m^2/yr) and coal-fired power plants Hg emissions (kg/yr)[128] in 2012.

Dataset S1 (separate file, SI Natural Archive Database.xlsx). Nature-archive mercury accumulation flux database 1700-2012, containing core information, references, and respective Hg accumulation flux data.

Dataset S2 (separate file, SI Monitoring data.xlsx). Ground monitoring of wet deposition and ambient concentration of mercury, containing location information and deposition flux data.

Dataset S3 (separate file, SI Figure Source Data.xlsx). The source data used to plot Figures 1-3 in the manuscript.

SI References

1. Cooke, C.A., et al., *Environmental archives of atmospheric Hg deposition – A review.* Science of The Total Environment, 2020. **709**: p. 134800.
2. Li, F., C. Ma, and P. Zhang, *Mercury Deposition, Climate Change and Anthropogenic Activities: A Review.* Frontiers in Earth Science, 2020. **8**.
3. Li, C., et al., *Unequal Anthropogenic Enrichment of Mercury in Earth's Northern and Southern Hemispheres.* ACS Earth and Space Chemistry, 2020. **4**(11): p. 2073-2081.
4. Engstrom, D.R., et al., *Atmospheric Hg Emissions from Preindustrial Gold and Silver Extraction in the Americas: A Reevaluation from Lake-Sediment Archives.* ENVIRONMENTAL SCIENCE & TECHNOLOGY, 2014. **48**(12): p. 6533-6543.
5. Goodsite, M.E., et al., *How well do environmental archives of atmospheric mercury deposition in the Arctic reproduce rates and trends depicted by atmospheric models and measurements?* Science of The Total Environment, 2013. **452-453**: p. 196-207.
6. Binford, M.W., *Calculation and uncertainty analysis of 210Pb dates for PIRLA project lake sediment cores.* Journal of Paleolimnology, 1990. **3**(3): p. 253-267.
7. Stuiver, M., et al., *INTCAL98 radiocarbon age calibration, 24,000–0 cal BP.* Radiocarbon, 1998. **40**(3): p. 1041-1083.
8. Gelaro, R., et al., *The modern-era retrospective analysis for research and applications, version 2 (MERRA-2).* Journal of climate, 2017. **30**(14): p. 5419-5454.
9. Selin, N.E., et al., *Global 3 -D land -ocean -atmosphere model for mercury: Present -day versus preindustrial cycles and anthropogenic enrichment factors for deposition.* Global biogeochemical cycles, 2008. **22**(2).
10. Schroeder, W.H. and J. Munthe, *Atmospheric mercury—An overview.* Atmospheric Environment, 1998. **32**(5): p. 809-822.
11. Selin, N.E., et al., *Chemical cycling and deposition of atmospheric mercury: Global constraints from observations.* Journal of Geophysical Research Atmospheres, 2007. **112**.
12. Sprovieri, F., et al., *Five-year records of mercury wet deposition flux at GMOS sites in the Northern and Southern hemispheres.* Atmos. Chem. Phys., 2017. **17**(4): p. 2689-2708.
13. Wesely, M.L., *Parameterization of surface resistances to gaseous dry deposition in regional-scale numerical models.* Atmospheric Environment, 1989. **23**(supp-S): p. 1293-1304.
14. Selin, N.E., *Global 3-D land-ocean-atmosphere model for mercury: Present-day versus preindustrial cycles and anthropogenic enrichment factors for deposition.* Global Biogeochemical Cycles, 2008. **22**.
15. Wesely, M.L. and B.B. Hicks, *A review of the current status of knowledge on dry deposition.* Atmospheric Environment, 2000. **34**(12): p. 2261-2282.
16. Zhang, L., J.R. Brook, and R. Vet, *A revised parameterization for gaseous dry deposition in air-quality models.* Atmos. Chem. Phys., 2003. **3**(6): p. 2067-2082.
17. Zhang, L., et al., *A Review of Dry Deposition Schemes for Speciated Atmospheric Mercury.* Bulletin of Environmental Contamination and Toxicology, 2023. **110**(1).
18. Zhou, J., et al., *Comparing ecosystem gaseous elemental mercury fluxes over a deciduous and coniferous forest.* Nature Communications, 2023. **14**(1).
19. Duan, L., et al., *Soil-atmosphere exchange of gaseous elemental mercury in three subtropical forests with different substrate Hg concentrations.* Atmospheric Environment, 2021. **244**.
20. Zhang, L., et al., *Atmospheric mercury deposition over the land surfaces and the associated uncertainties in observations and simulations: a critical review.* ATMOSPHERIC CHEMISTRY AND PHYSICS, 2019. **19**(24): p. 15587-15608.
21. Sommar, J., S. Osterwalder, and W. Zhu, *Recent advances in understanding and measurement of Hg in the environment: Surface-atmosphere exchange of gaseous elemental mercury (Hg).* Science of the Total Environment, 2020. **721**.
22. Zhu, W., et al., *Global observations and modeling of atmosphere-surface exchange of elemental mercury: a critical review.* Atmospheric Chemistry and Physics, 2016. **16**(7): p. 4451-4480.
23. Yu, K., et al., *Errors and improvements in the use of archived meteorological data for chemical transport modeling: an analysis using GEOS-Chem v11-01 driven by GEOS-5 meteorology.* Geosci. Model Dev., 2018. **11**(1): p. 305-319.
24. Horowitz, H.M., et al., *A new mechanism for atmospheric mercury redox chemistry: implications for the global mercury budget.* Atmos. Chem. Phys., 2017. **17**(10): p. 6353-6371.
25. Liu, K., et al., *Measure-Specific Effectiveness of Air Pollution Control on China's Atmospheric Mercury Concentration and Deposition during 2013–2017.* Environmental Science & Technology, 2019. **53**(15): p. 8938-8946.
26. Larsen, K., *GAM: The Predictive Modeling Silver Bullet*. 2015.
27. Muntean, M., et al., *Evaluating EDGARv4.tox2 speciated mercury emissions ex-post scenarios and their impacts on modelled global and regional wet deposition patterns.* Atmospheric Environment, 2018. **184**: p. 56-68.
28. Menard, S., *Applied logistic regression analysis*. 2002: Sage.
29. Gareth, J., et al., *An introduction to statistical learning: with applications in R*. 2013: Springer.
30. McCullagh, P. and J. Nelder, *Generalized linear models*. 1989: Chapman and Hill.
31. Hastie, T., et al., *The elements of statistical learning: data mining, inference, and prediction*. Vol. 2. 2009: Springer.
32. DataCamp, *CVgam: Cross-validation estimate of accuracy from GAM model fit*. gamclass (version 0.62.3) 2020.

33. Pedersen, E.J., et al., *Hierarchical generalized additive models in ecology: an introduction with mgcv.* PeerJ, 2019. **7**: p. e6876.
34. Gilbert, R.O., *Statistical methods for environmental pollution monitoring*. 1987: John Wiley & Sons.
35. Streets, D.G., et al., *Total Mercury Released to the Environment by Human Activities.* Environmental Science & Technology, 2017. **51**(11): p. 5969-5977.
36. UNEP, *Global Mercury Assessment 2018*. 2019.
37. Matsumura, K., K. Kawase, and K. Takeya, *Observation of sublimation of ice using terahertz spectroscopy.* Royal Society Open Science, 2020. **7**(9): p. 192083.
38. Huang, J., et al., *Spatial distribution and magnification processes of mercury in snow from high-elevation glaciers in the Tibetan Plateau.* Atmospheric Environment, 2012. **46**: p. 140-146.
39. DiMento, B.P., et al., *The impact of sea ice on the air-sea exchange of mercury in the Arctic Ocean.* Deep Sea Research Part I: Oceanographic Research Papers, 2019. **144**: p. 28-38.
40. Overeem, I., et al., *Substantial export of suspended sediment to the global oceans from glacial erosion in Greenland.* Nature Geoscience, 2017. **10**(11): p. 859-863.
41. Fox-Kemper, B., H.T. Hewitt, C. Xiao, G. Aðalgeirsdóttir, S.S. Drijfhout, T.L. Edwards, N.R. Golledge, M. Hemer, R.E. Kopp, G. Krinner, A. Mix, D. Notz, S. Nowicki, I.S. Nurhati, L. Ruiz, J.-B. Sallée, A.B.A. Slangen, and Y. Yu, *Ocean, Cryosphere and Sea Level Change*. Climate Change 2021: The Physical Science Basis. Contribution of Working Group I to the Sixth Assessment Report of the Intergovernmental Panel on Climate Change, ed. V. Masson-Delmotte, P. Zhai, A. Pirani, S.L. Connors, C. Péan, S. Berger, N. Caud, Y. Chen, L. Goldfarb, M.I. Gomis, M. Huang, K. Leitzell, E. Lonnoy, J.B.R. Matthews, T.K. Maycock, T. Waterfield, O. Yelekçi, R. Yu, and B. Zhou. 2021, Cambridge, United Kingdom and New York, NY, USA. 1211–1362.
42. Meng, M., et al., *An Integrated Model for Input and Migration of Mercury in Chinese Coastal Sediments.* Environmental Science & Technology, 2019. **53**(5): p. 2460-2471.
43. Loranty, M.M., et al., *Spatial variation in vegetation productivity trends, fire disturbance, and soil carbon across arctic-boreal permafrost ecosystems.* ENVIRONMENTAL RESEARCH LETTERS, 2016. **11**(9).
44. Trombetta, T., et al., *Water temperature drives phytoplankton blooms in coastal waters.* PLOS ONE, 2019. **14**(4).
45. Zhang, Y., et al., *An updated global mercury budget from a coupled atmosphere-land-ocean model: 40% more re-emissions buffer the effect of primary emission reductions.* One Earth, 2023. **6**(3): p. 316-325.
46. Zhou, J., et al., *Vegetation uptake of mercury and impacts on global cycling.* Nature Reviews Earth & Environment, 2021. **2**(4): p. 269-284.
47. Southworth, G., et al., *Evasion of added isotopic mercury from a northern temperate lake.* Environmental Toxicology and Chemistry: An International Journal, 2007. **26**(1): p. 53-60.
48. Yang, H., D.R. Engstrom, and N.L. Rose, *Recent Changes in Atmospheric Mercury Deposition Recorded in the Sediments of Remote Equatorial Lakes in the Rwenzori Mountains, Uganda.* Environmental Science & Technology, 2010. **44**(17): p. 6570-6575.
49. Creed, I.F., et al., *Global change-driven effects on dissolved organic matter composition: Implications for food webs of northern lakes.* GLOBAL CHANGE BIOLOGY, 2018. **24**(8): p. 3692-3714.
50. Rydberg, J., et al., *Climate driven release of carbon and mercury from permafrost mires increases mercury loading to sub-arctic lakes.* Science of The Total Environment, 2010. **408**(20): p. 4778-4783.
51. Cooke, C.A., et al., *A Holocene Perspective on Algal Mercury Scavenging to Sediments of an Arctic Lake.* ENVIRONMENTAL SCIENCE & TECHNOLOGY, 2012. **46**(13): p. 7135-7141.
52. Zhu, T., et al., *Accumulation of Pollutants in Proglacial Lake Sediments: Impacts of Glacial Meltwater and Anthropogenic Activities.* Environmental Science & Technology, 2020. **54**(13): p. 7901-7910.
53. Perez-Rodriguez, M., et al., *Thawing of snow and ice caused extraordinary high and fast mercury fluxes to lake sediments in Antarctica.* GEOCHIMICA ET COSMOCHIMICA ACTA, 2019. **248**: p. 109-122.
54. Sun, X., et al., *Melting Himalayas and mercury export: Results of continuous observations from the Rongbuk Glacier on Mt. Everest and future insights.* Water Research, 2022. **218**: p. 118474.
55. Verbeke, B.A., et al., *Latitude, elevation, and mean annual temperature predict peat organic matter chemistry at a global scale.* Global Biogeochemical Cycles, 2022. **36**(2): p. e2021GB007057.
56. Biester, H., et al., *Effect of peat decomposition and mass loss on historic mercury records in peat bogs from Patagonia.* Environmental science & technology, 2003. **37**(1): p. 32-39.
57. Sirota, J.I., et al., *Mercury dynamics in the pore water of peat columns during experimental freezing and thawing.* JOURNAL OF ENVIRONMENTAL QUALITY, 2020. **49**(2): p. 404-416.
58. Martínez-Cortizas, A., et al., *Mercury in a Spanish Peat Bog: Archive of Climate Change and Atmospheric Metal Deposition.* Science, 1999. **284**(5416): p. 939-942.
59. Yee, Y.H., et al., *SUBCATCHMENT OUTPUT OF MERCURY AND METHYLMERCURY AT SVARTBERGET IN NORTHERN SWEDEN.* WATER AIR AND SOIL POLLUTION, 1995. **80**(1-4): p. 455-465.
60. Thiagarajan, N. and J.F. McManus, *Productivity and sediment focusing in the Eastern Equatorial Pacific during the last 30,000 years.* Deep Sea Research Part I: Oceanographic Research Papers, 2019. **147**: p. 100-110.
61. Martin, J., et al., *Recent accumulation of trace metals in sediments at the DYFAMED site (Northwestern Mediterranean Sea).* MARINE POLLUTION BULLETIN, 2009. **59**(4-7): p. 146-153.
62. Cossa, D., et al., *Mediterranean Mercury Assessment 2022: An Updated Budget, Health Consequences, and Research Perspectives.* Environmental Science & Technology, 2022. **56**(7): p. 3840-3862.
63. Lamborg, C.H., et al., *A global ocean inventory of anthropogenic mercury based on water column measurements.* Nature, 2014. **512**(7512): p. 65-68.
64. Weigelt, A., et al., *Tropospheric mercury vertical profiles between 500 and 10 000 m in central Europe.* Atmospheric Chemistry and Physics, 2016. **16**(6): p. 4135-4146.

65. Yang, H., et al., *Historical Reconstruction of Mercury Pollution Across the Tibetan Plateau Using Lake Sediments.* Environmental Science & Technology, 2010. **44**(8): p. 2918-2924.
66. Zheng, J., *Archives of total mercury reconstructed with ice and snow from Greenland and the Canadian High Arctic.* Science of the Total Environment, 2015. **509**: p. 133-144.
67. Guo, D., E. Yu, and H. Wang, *Will the Tibetan Plateau warming depend on elevation in the future?* Journal of Geophysical Research: Atmospheres, 2016. **121**(8): p. 3969-3978.
68. Pepin, N., et al., *An Examination of Temperature Trends at High Elevations Across the Tibetan Plateau: The Use of MODIS LST to Understand Patterns of Elevation-Dependent Warming.* Journal of Geophysical Research: Atmospheres, 2019. **124**(11): p. 5738-5756.
69. Khan, A., S.M. Haque, and B. Biswas, *Altitudinal Shifting of Apple Orchards with Adaption of Changing Climate in the Alpine Himalaya.* Journal of the Indian Society of Remote Sensing, 2023. **51**(5): p. 1135-1155.
70. Sanz‐Elorza, M., et al., *Changes in the High‐mountain Vegetation of the Central Iberian Peninsula as a Probable Sign of Global Warming.* Annals of Botany, 2003. **92**(2): p. 273-280.
71. Streets, D.G., et al., *Global and regional trends in mercury emissions and concentrations, 2010–2015.* Atmospheric Environment, 2019. **201**: p. 417-427.
72. Verbrugge, B. and S. Geenen, *Global Gold Production Touching Ground: Expansion, Informalization, and Technological Innovation*. 2020, Cham: Springer International Publishing: Cham.
73. Biester, H., et al., *Modeling the Past Atmospheric Deposition of Mercury Using Natural Archives.* Environmental Science & Technology, 2007. **41**(14): p. 4851-4860.
74. Chellman, N., et al., *Reassessment of the Upper Fremont Glacier Ice-Core Chronologies by Synchronizing of Ice-Core-Water Isotopes to a Nearby Tree-Ring Chronology.* Environmental Science & Technology, 2017. **51**(8): p. 4230-4238.
75. Schuster, P.F., et al., *Atmospheric mercury deposition during the last 270 years: A glacial ice core record of natural and anthropogenic sources.* ENVIRONMENTAL SCIENCE & TECHNOLOGY, 2002. **36**(11): p. 2303-2310.
76. Janssens-Maenhout, G., et al., *Global emission inventories in the Emission Database for Global Atmospheric Research (EDGAR)–Manual (I).* Gridding: EDGAR emissions distribution on global gridmaps, Publications Office of the European Union, Luxembourg, 2013. **775**.
77. Rossmann, R., *Protocol to Reconstruct Historical Contaminant Loading to Large Lakes: The Lake Michigan Sediment Record of Mercury.* Environmental Science & Technology, 2010. **44**(3): p. 935-940.
78. Fitzgerald, W.F., et al., *Modern and historic atmospheric mercury fluxes in northern Alaska: Global sources and Arctic depletion.* Environmental science & technology, 2005. **39**(2): p. 557-568.
79. Streets, D.G., et al., *All-Time Releases of Mercury to the Atmosphere from Human Activities.* Environmental Science & Technology, 2011. **45**(24): p. 10485-10491.
80. Camargo, J.A., *Contribution of Spanish–American silver mines (1570–1820) to the present high mercury concentrations in the global environment: a review.* Chemosphere, 2002. **48**(1): p. 51-57.
81. AMAP/UNEP, *Technical Background Report for the Global Mercury Assessment 2018*. 2019, Arctic Monitoring and Assessment Programme, Oslo, Norway/UN Environment Programme, Chemicals and Health Branch, Geneva, Switzerland.
82. Zhang, Y., et al., *Six centuries of changing oceanic mercury.* Global Biogeochemical Cycles, 2014. **28**(11): p. 1251-1261.
83. Guerrero, S. and L. Schneider, *The global roots of pre-1900 legacy mercury.* Proceedings of the National Academy of Sciences, 2023. **120**(31): p. e2304059120.
84. Streets, D.G., et al., *Five hundred years of anthropogenic mercury: spatial and temporal release profiles.* ENVIRONMENTAL RESEARCH LETTERS, 2019. **14**(8).
85. Gerson, J.R., et al., *Amazon forests capture high levels of atmospheric mercury pollution from artisanal gold mining.* Nature Communications, 2022. **13**(1): p. 559.
86. Roberts, S.L., et al., *Quantification of Spatial and Temporal Trends in Atmospheric Mercury Deposition across Canada over the Past 30 Years.* Environmental Science & Technology, 2021. **55**(23): p. 15766-15775.
87. Martin, A., *Uncovered The dark world of the Zama Zamas*. 2019.
88. Grynberg, R. and F. Singogo, *The ASGM Sector in Africa: Lessons from China*. 2021. p. 49-109.
89. Rose, N.L., et al., *Natural archives of long-range transported contamination at the remote lake Letšeng-la Letsie, Maloti Mountains, Lesotho.* Science of The Total Environment, 2020. **737**: p. 139642.
90. Kirk, J.L., V.L. St. Louis, and M.J. Sharp, *Rapid reduction and reemission of mercury deposited into snowpacks during atmospheric mercury depletion events at Churchill, Manitoba, Canada.* Environmental science & technology, 2006. **40**(24): p. 7590-7596.
91. Moore, C.W., et al., *Convective forcing of mercury and ozone in the Arctic boundary layer induced by leads in sea ice.* Nature, 2014. **506**(7486): p. 81-84.
92. Steffen, A., et al., *Atmospheric mercury over sea ice during the OASIS-2009 campaign.* ATMOSPHERIC CHEMISTRY AND PHYSICS, 2013. **13**(14): p. 7007-7021.
93. Kang, S., et al., *Atmospheric Mercury Depositional Chronology Reconstructed from Lake Sediments and Ice Core in the Himalayas and Tibetan Plateau.* Environmental Science & Technology, 2016. **50**(6): p. 2859-2869.
94. Norton, S.A., et al., *A comparative study of long-term Hg and Pb sediment archives.* Environmental Chemistry, 2016. **13**(3): p. 517-527.
95. Rausch, N., et al., *Retention of atmospheric Cu, Ni, Cd and Zn in an ombrotrophic peat profile near the Outokumpu Cu-Ni mine, SE-Finland.* JOURNAL DE PHYSIQUE IV, 2003. **107**: p. 1127-1130.
96. Moore, T.R., et al., *Methyl and Total Mercury in Boreal Wetland Plants, Experimental Lakes Area, Northwestern Ontario.* Journal of Environmental Quality, 1995. **24**(5): p. 845-850.

97. Miszczak, E., et al., *A novel approach to peatlands as archives of total cumulative spatial pollution loads from atmospheric deposition of airborne elements complementary to EMEP data: priority pollutants (Pb, Cd, Hg).* SCIENCE OF THE TOTAL ENVIRONMENT, 2020. **705**.
98. Norton, S.A., G.C. Evans, and J.S. Kahl, *Comparison of Hg and Pb Fluxes to Hummocks and Hollows of Ombrotrophic Big Heath Bog and to Nearby Sargent Mt. Pond, Maine, USA.* Water, Air, and Soil Pollution, 1997. **100**(3): p. 271-286.
99. Ettler, V., et al., *Mercury deposition/accumulation rates in the vicinity of a lead smelter as recorded by a peat deposit.* Atmospheric Environment, 2008. **42**(24): p. 5968-5977.
100. Wasik, J.K.C., et al., *The effects of hydrologic fluctuation and sulfate regeneration on mercury cycling in an experimental peatland.* JOURNAL OF GEOPHYSICAL RESEARCH-BIOGEOSCIENCES, 2015. **120**(9): p. 1697-1715.
101. Osterwalder, S., et al., *Mercury evasion from a boreal peatland shortens the timeline for recovery from legacy pollution.* Scientific Reports, 2017. **7**(1): p. 16022.
102. Fritsche, J., et al., *Evasion of Elemental Mercury from a Boreal Peat land Suppressed by Long-Term Sulfate Addition.* ENVIRONMENTAL SCIENCE & TECHNOLOGY LETTERS, 2014. **1**(10): p. 421-425.
103. Novak, M., et al., *Isotopic evidence for nitrogen mobility in peat bogs.* GEOCHIMICA ET COSMOCHIMICA ACTA, 2014. **133**: p. 351-361.
104. Bandara, S., et al., *Postdepositional Mercury Mobility in a Permafrost Peatland from Central Yukon, Canada.* ACS EARTH AND SPACE CHEMISTRY, 2019. **3**(5): p. 770-778.
105. Korosi, J.B., et al., *Trends in historical mercury deposition inferred from lake sediment cores across a climate gradient in the Canadian High Arctic.* Environmental Pollution, 2018. **241**: p. 459-467.
106. Evenset, A., et al., *Historical trends in persistent organic pollutants and metals recorded in sediment from Lake Ellasjøen, Bjørnøya, Norwegian Arctic.* Environmental Pollution, 2007. **146**(1): p. 196-205.
107. Kamman, N.C. and D.R. Engstrom, *Historical and present fluxes of mercury to Vermont and New Hampshire lakes inferred from 210Pb dated sediment cores.* Atmospheric Environment, 2002. **36**(10): p. 1599-1609.
108. Ribeiro Guevara, S., et al., *Sediment records of highly variable mercury inputs to mountain lakes in Patagonia during the past millennium.* Atmos. Chem. Phys., 2010. **10**(7): p. 3443-3453.
109. Shotbolt, L.A., A.D. Thomas, and S.M. Hutchinson, *The use of reservoir sediments as environmental archives of catchment inputs and atmospheric pollution.* Progress in Physical Geography, 2005. **29**(3): p. 337-361.
110. Wiklund, J.A., et al., *Anthropogenic mercury deposition in Flin Flon Manitoba and the Experimental Lakes Area Ontario (Canada): A multi-lake sediment core reconstruction.* Science of The Total Environment, 2017. **586**: p. 685-695.
111. Lent, R.M. and C.R. Alexander, *Mercury accumulation in Devils Lake, North Dakota — Effects of environmental variation in closed-basin lakes on mercury chrologies.* Water, Air, and Soil Pollution, 1997. **98**(3): p. 275-296.
112. Fitzgerald, W.F., et al., *Modern and historic atmospheric mercury fluxes in northern Alaska: Global sources and Arctic depletion.* ENVIRONMENTAL SCIENCE & TECHNOLOGY, 2005. **39**(2): p. 557-568.
113. Fitzgerald, W.F., et al., *Modern and Historic Atmospheric Mercury Fluxes in Northern Alaska: Global Sources and Arctic Depletion.* Environmental Science & Technology, 2005. **39**(2): p. 557-568.
114. Lehman, J.T., *Reconstructing the Rate of Accumulation of Lake Sediment: The Effect of Sediment Focusing1*. Quaternary Research, 1975. **5**(4): p. 541-550.
115. Liu, M.D., et al., *Rivers as the largest source of mercury to coastal oceans worldwide.* NATURE GEOSCIENCE, 2021. **14**(9): p. 672-+.
116. Dastoor, A., et al., *Arctic mercury cycling.* Nature Reviews Earth & Environment, 2022. **3**(4): p. 270-286.
117. Asmund, G. and S.P. Nielsen, *Mercury in dated Greenland marine sediments.* Science of The Total Environment, 2000. **245**(1): p. 61-72.
118. Abril, G., et al., *Turbidity limits gas exchange in a large macrotidal estuary.* ESTUARINE COASTAL AND SHELF SCIENCE, 2009. **83**(3): p. 342-348.
119. Outridge, P.M., et al., *Updated global and oceanic mercury budgets for the United Nations Global Mercury Assessment 2018.* Environmental science & technology, 2018. **52**(20): p. 11466-11477.
120. USGS, *Space Shuttle Radar Topography Mission (SRTM)*. 2000.
121. Bosilovich, M.G., *MERRA-2: Initial evaluation of the climate*. 2015: National Aeronautics and Space Administration, Goddard Space Flight Center.
122. Koster, R.D., et al., *MERRA-2 input observations: Summary and assessment*. 2016.
123. Muntean, M., et al., *Trend analysis from 1970 to 2008 and model evaluation of EDGARv4 global gridded anthropogenic mercury emissions.* Science of The Total Environment, 2014. **494-495**: p. 337-350.
124. bp, *bp Statistical Review of World Energy - all data*. 2022.
125. World Bank, *GNI per capita, Atlas method (current US$)*, in *annum*. 2022.
126. Thomson Reuters, *GFMS Gold Survey 2018*. 2020.
127. Rose, N.L., et al., *Natural archives of long-range transported contamination at the remote lake Letšeng-la Letsie, Maloti Mountains, Lesotho.* Science of The Total Environment, 2020. **737**: p. 139642.
128. Oberschelp, C., et al., *Global emission hotspots of coal power generation.* Nature Sustainability, 2019. **2**(2): p. 113-121.